

Effects of wave-induced forcing on a circulation model of the North Sea

Joanna Staneva¹ · Victor Alari^{1,2} · Øyvind Breivik³ ·
Jean-Raymond Bidlot⁴ · Kristian Mogensen⁴

Received: 17 May 2016 / Accepted: 4 October 2016 / Published online: 19 November 2016
© Springer-Verlag Berlin Heidelberg 2016

Abstract The effect of wind waves on water level and currents during two storms in the North Sea is investigated using a high-resolution Nucleus for European Modelling of the Ocean (NEMO) model forced with fluxes and fields from a high-resolution wave model. The additional terms accounting for wave-current interaction that are considered in this study are the Stokes-Coriolis force, the sea-state-dependent energy and momentum fluxes. The individual and collective role of these processes is quantified and the results are compared with a control run without wave effects as well as against current and water-level measurements from coastal stations. We find a better agreement with observations when the circulation model is forced by sea-state-dependent fluxes, especially in extreme events. The two extreme events, the storm Christian (25–27 October 2013), and about a month later, the storm Xaver (5–7 December 2013), induce different wave and surge conditions over the North Sea. Including the wave effects in

the circulation model for the storm Xaver raises the modelled surge by more than 40 cm compared with the control run in the German Bight area. For the storm Christian, a difference of 20–30 cm in the surge level between the wave-forced and the stand-alone ocean model is found over the whole southern part of the North Sea. Moreover, the modelled vertical velocity profile fits the observations very well when the wave forcing is accounted for. The contribution of wave-induced forcing has been quantified indicating that this represents an important mechanism for improving water-level and current predictions.

Keywords Wave-current interaction · NEMO · WAM · North Sea · Surge predictions · Coastal forecasts · Stokes drift

1 Introduction

Accurate water-level forecasting remains a challenging topic in coastal flooding research, not least along the European shelf which is characterised by vast shallow tidal flats and a large coastal population. The increased demand for improved water-level predictions requires further development and refinement of the physical processes represented by the hydrodynamical models to properly account for wave-generated currents and the corresponding changes to the water level. That the wind-induced surface stress plays an important role in shallow-water regions has been demonstrated by many previous studies (e.g. Flather 2001).

The importance of wave-generated turbulence near the sea surface has been demonstrated by Davies et al. (2000), for the bottom layer by Jones and Davies (1998) and for wave-induced turbulence by Babanin (2006). Huang et al. (2011) parameterised the TKE dissipation rate due to wave-turbulence interactions. Based on laboratory (Babanin and Haus 2009) and

This article is part of the Topical Collection on the *14th International Workshop on Wave Hindcasting and Forecasting in Key West, Florida, USA, November 8–13, 2015*

Responsible Editor: Diana Greenslade

✉ Joanna Staneva
joanna.staneva@hzg.de

¹ Institute for Coastal Research, Helmholtz-Zentrum Geesthacht, Max-Planck Strasse 1, 21502 Geesthacht, Germany

² Marine Systems Institute, Tallinn University of Technology, Akadeemia tee 15a, 12611 Tallinn, Estonia

³ Norwegian Meteorological Institute and Geophysical Institute, University of Bergen, Bergen, Norway

⁴ European Centre for Medium-Range Weather Forecasts (ECMWF), Shinfield Park, Reading RG2 9AX, UK

numerical results (Babanin and Chalikov 2012), Babanin (2011) showed that the major sink for swell energy is oceanic turbulence while Janssen (2012) demonstrated a positive impact of wave breaking on the daily cycle of sea-surface temperature.

The potential impact of waves on the representation of the ocean surface boundary layer in ocean models has recently triggered a renewed interest on the various ways in which the oceanic wave field may affect upper-ocean currents, water level and hydrography. The seminal study by Longuet-Higgins and Stewart (1961, 1962, 1964) more than 50 years ago showed that wave shoaling and breaking would set up gradients of radiation stress that represent a transfer of wave momentum to the water column that forces a change in the mean water level. The effects of waves on the atmospheric boundary layer were demonstrated by a number of studies (Janssen 1989, 1991; Donelan et al. 2012; Fan et al. 2009). The effects of wave-current interactions caused by radiation stresses were also shown by Brown and Wolf (2009). Weber et al. (2006) found that the Eulerian and Lagrangian approaches to the wave-induced transport in the upper ocean produce the same mean wave-induced flux in the surface layer and that the wave-induced stress constituted about 50 % of the total atmospheric stress for moderate to strong winds. Many other studies based on theoretical and practical analyses have demonstrated the impact waves have on the upper ocean (Mellor 2003, 2005, 2008; Ardhuin et al. 2008, 2010; Kumar et al. 2012; Michaud et al. 2012). Mellor (2003, 2005, 2008) extended the radiation stress formulation based on the linear wave theory of Longuet-Higgins and Stewart (1964). Bennis and Ardhuin (2011) questioned the method of Mellor and suggested the use of Lagrangian mean framework leading to the so-called vortex force. The vortex force method has been utilised in a series of studies (e.g. Kumar et al. 2012; Lane et al. 2007; McWilliams et al. 2004; Uchiyama et al. 2010; Barbariol et al. 2013; Benetazzo et al. 2013). Moghimi et al. (2013) compared critically the two approaches claiming that the radiation stress formulation showed unrealistic offshore-directed transport in the wave shoaling regions. On the other hand, the results of longshore circulations performed similarly for both methods. Aiki and Greatbatch (2013, 2014) proved that the radiation stress formulation of Mellor is applicable for small bottom slopes. The importance of wave-current interactions in a tidally dominated estuary has been demonstrated by Bolaños et al. (2011, 2014) who found that the inclusion of wave effects through 3D radiation stress improves the current velocity in the study area. They also compared the different radiation stress methods and concluded that for the tidally dominated area, the 3D version of radiation stress produces better results than the 2D version. Polton et al. (2005) showed that accounting for the Stokes-Coriolis forcing results in encouraging agreement between model and measurements of the mixed layer. Babanin et al. (2010) found that the main effects of waves on the mean flow are due to

radiation stress and Stokes drift, although interaction with turbulence and bottom stress can also be important. By analysing high-frequency (HF) radar observations, Ardhuin et al. (2009) demonstrated that the Stokes drift is between 0.6 and 1.3 % of the wind speed and of similar magnitude as the direct wind-induced current (that is 1–1.8 % of the wind speed).

Breivik et al. (2015) demonstrated reduced bias between modelled and measured water temperature by incorporating the Stokes-Coriolis forcing and fluxes of turbulent kinetic energy and momentum (wave-modulated stress) from a wave model in a global-scale Nucleus for European Modelling of the Ocean (NEMO) model. This work was later adapted to a regional NEMO model for the Baltic and North Sea by Alari et al. (2015).

The role of waves on Lagrangian particle transport has been investigated by Röhrs et al. (2012, 2014). Adding the Stokes-Coriolis force to the momentum equations significantly affects the Ekman spiral (Polton et al. 2005). In addition, there is also the direct effect of the Stokes drift on the object. Röhrs et al. (2015) used HF radar measurements to further demonstrate the importance of properly accounting for waves in Lagrangian drifter studies by comparing current measurements from HF radars and Acoustic Doppler Current Profilers (ADCP) against drifter-derived currents. They found that a significant difference stemming from the added Stokes drift in the drifter data (the HF radar currents were found to be unaffected by Stokes drift and can thus be considered a Eulerian current estimate). As breaking commences, the wave energy and momentum decreases, resulting in a reduction of the radiation stress carried by the waves. These stresses are important in coastal areas as they force a rise in mean sea level.

The impact of waves on water level under hurricane conditions in the Gulf of Mexico and a storm in the Adriatic Sea was demonstrated by Roland et al. (2009) and for storm conditions in the Irish Sea by Brown et al. (2011) and Brown and Wolf (2009). For the Irish Sea, the role of wave-current interaction has also been studied by Wolf et al. (2011), Brown et al. (2013) and Katsafados et al. (2016). It has been shown that often in wave-influenced estuaries the wave related processes are greater during high water when wave dissipation over the banks at the mouth is smaller. The timing of the wave conditions relative to the tidal flow at the estuary mouth is thus also relevant to the sediment dynamics. During storm events, the waves can significantly modulate the storm surge. According to Dean and Dalrymple (1991) the effective change in water level from a steady train of linear waves approaching normal to the shore on a gently sloping bottom is about 19 % of the breaking wave height. This may increase or decrease as we take into account nonlinear effects, dissipative forces, and wave obliquity. The amount of wave setup is also affected by the bottom contour of the near-shore and beach face. Moreover, the contribution of the short waves in storm surges is demonstrated by Bertin et al. (2015). They studied the contribution of wave-enhanced surface and bottom stresses and

the gradients of the radiation stress. The first proper wave-storm surge model was set up by Mastenbroek et al. (1993). They demonstrated a modest increase in the water level under storm conditions in the North Sea when a wave-induced drag and radiation stresses were incorporated in the WAQUA hydrodynamics model. Saetra et al. (2007) likewise showed the importance of properly accounting for waves in a three-dimensional model of the North Sea.

In this paper, we examine the effect of wave-current interaction in the North Sea for two storm events aiming at further increasing our understanding of the role that waves play in building storm surges under extreme conditions. We investigate two storms that occurred in late 2013, Christian (25–27 October 2013) and about 40 days later the storm Xaver (5–7 December 2013).

The structure of the paper is as follows. In Sect. 2, we describe the wave and hydrodynamic models, their setup in this study as well as the atmospheric conditions in the period of the two extreme events. This is followed by a detailed description of the observational data used. Section 3 discusses the wave effects introduced into the ocean model, namely the Stokes–Coriolis forcing, the sea-state-dependent fluxes of turbulent kinetic energy and momentum from breaking waves. We then present the sensitivity experiments performed. The performance of the wave and circulation model, including a discussion of the role of the wave effects on the surge and circulation for the period of study, is presented in Sect. 4. Finally, we summarise the main findings of the study and point to future developments in this field (Sect. 5).

2 Methods

2.1 Circulation model NEMO

NEMO (Madec et al. 2008) is a framework of ocean-related computing engines, from which we use the OPA package (for the ocean dynamics and thermodynamics) and the LIM2 sea-ice dynamics and thermodynamics package (Madec et al. 2008; Bouillon et al. 2009). In OPA, six primitive equations (momentum balance, the hydrostatic equilibrium, the incompressibility equation, the heat and salt conservation equations and an equation of state) are solved, where the Arakawa C grid is used in the horizontal. In the vertical, terrain-following coordinates, z coordinates or hybrid z - s coordinates can be used. For a complete description of the model, see Madec (2008). Previously, NEMO has been applied to the Baltic Sea and the North Sea area in uncoupled mode (Hordoir et al. 2013), coupled to atmospheric models (Dieterich et al. 2013; Pham et al. 2014) and forced with a wave model (Alari et al. 2015). For the north-western European shelf, NEMO is used as a forecasting model in the COPERNICUS Marine Services (O’Dea et al. 2012; Siddorn et al. 2016).

2.2 Wave model WAM

The wave model WAM (The WAMDI Group 1988; ECMWF 2014) is a third-generation wave model, which solves the action balance equation without any a priori restriction on the evolution of spectrum. The wave action density spectrum N is considered instead of the energy density spectrum E because in the presence of ambient currents, action density is conserved, but energy density is not. Action density is related to energy density through the relative frequency (Whitham 1974; Komen et al. 1994):

$$N(\sigma, \theta) = \frac{E(\sigma, \theta)}{\sigma} \tag{1}$$

The variable σ is the relative frequency (as observed in a frame of reference moving with the current velocity) and θ is the wave direction (the direction normal to the wave crest of each spectral component). The action balance equation in Cartesian coordinates reads:

$$\begin{aligned} \frac{\partial N}{\partial t} + (\mathbf{c}_g + \mathbf{U}) \nabla_{x,y} N + \frac{\partial c_\sigma N}{\partial \sigma} + \frac{\partial c_\theta N}{\partial \theta} \\ = \frac{S_{\text{wind}} + S_{\text{nl4}} + S_{\text{wc}} + S_{\text{bot}} + S_{\text{br}}}{\sigma} \end{aligned} \tag{2}$$

On the left-hand side of Eq. (2), the first term represents the local rate of change of action density in time; the second one denotes the propagation of wave energy in two-dimensional geographical space, where \mathbf{c}_g is the group velocity vector and \mathbf{U} the ambient current vector. The third term represents shifting of the relative frequency due to variations in depths and currents (with propagation velocity c_σ in σ space). The fourth term represents depth- and current-induced refractions (with propagation velocity c_θ in θ space). On the right-hand side of the action balance equation is the source term that represents physical processes which generate, redistribute or dissipate wave energy in the WAM model. These terms denote, respectively, wave growth by the wind (S_{wind}), nonlinear transfer of wave energy through four-wave interactions (S_{nl4}) and wave dissipation caused by white capping (S_{wc}) and bottom friction (S_{bot}). In the present calculations, we also took into account depth-induced wave breaking (S_{br}).

The last release of the third-generation wave model WAM Cycle 4.5.4 is an update of the WAM Cycle 4 wave model, which is described in Komen et al. (1994) and Günther et al. (1992). The basic physics and numerics are kept in the new release. The source function integration scheme is made by Hersbach and Janssen (1999), and the updated source terms of Bidlot et al. (2007) are incorporated.

2.3 Model setup

NEMO and WAM share the same computational grid and bathymetry with a horizontal resolution of 2 nautical miles

covering the Baltic Sea and the North Sea. Here, we focus on the North Sea (Fig. 1). In the vertical, NEMO was set up with 56 z levels. The spectrum in WAM was discretised with 24 directions and 25 frequencies. The hourly atmospheric forcing is taken from subsequent short-range forecasts from the regional atmospheric model COSMO-EU, operated by the German Weather Service (DWD). The horizontal resolution is 7 km on a domain that covers the whole of Europe. The model has 40 vertical levels up to about 24 km. The horizontal resolution enables COSMO-EU to resolve small-scale features due to topographically induced flow which have a pronounced impact on the coastal weather in the North Sea region, such as land-sea breezes and channelling of the flow in the upper Rhine valley (https://www.dwd.de/EN/research/weatherforecasting/num_modelling/01_num_weather_prediction_modells/regional_model_cosmo_eu.html).

The required boundary information used at the open boundaries of the North Sea model is taken from the regional wave model EWAM for Europe, which is run twice a day in operational wave forecast routine at DWD. The open boundaries of the models are located in the western part of the

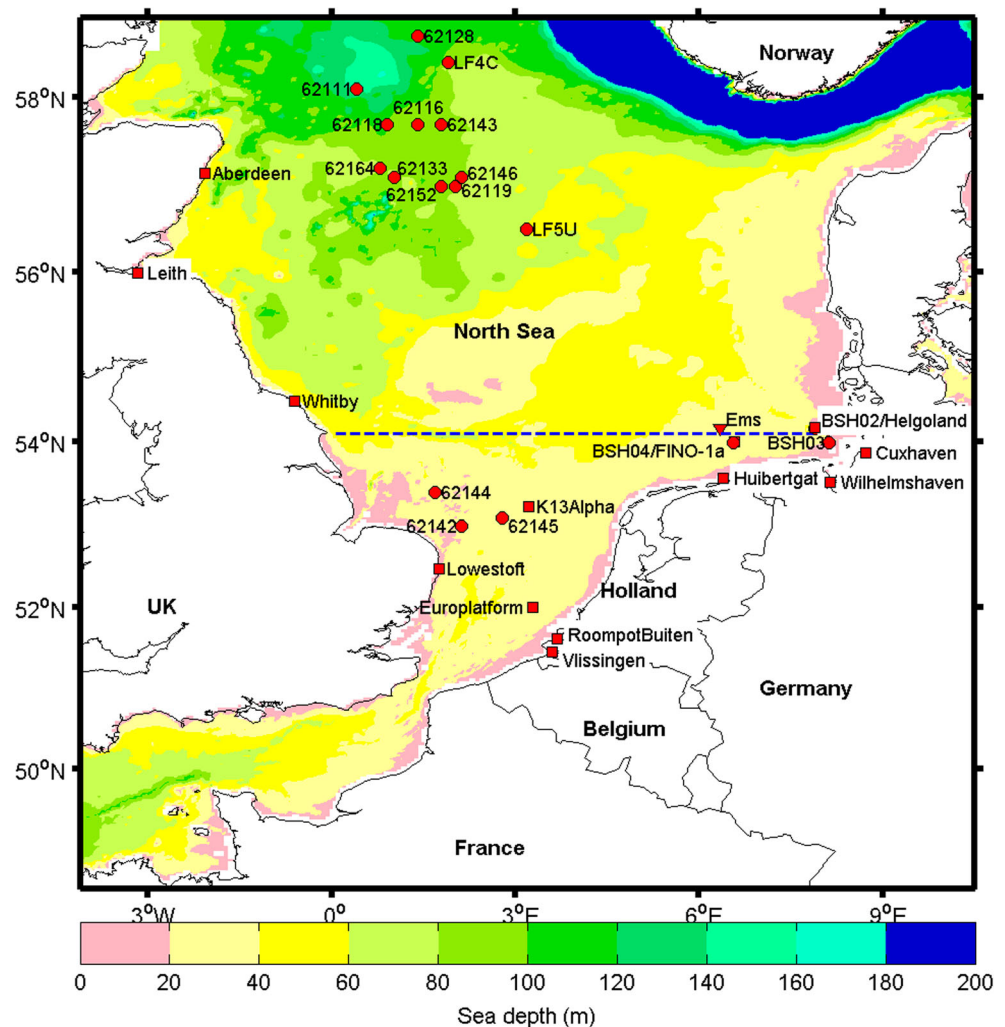
English Channel and near the continental shelf break of the North Sea. At the open boundaries, tidal amplitudes and velocities are prescribed as well as climatological temperature and salinity. As for the initial conditions, the wave model starts from rest, while the ocean model uses the climatology by Janssen et al. (1999). In this study, the analysed period is from October to December 2013.

In WAM, the source term integration time step was 60 s and the propagation time step was 10 s. In the circulation model NEMO, the baroclinic time step was 180 s and the barotropic one 10 s. The z levels had a vertical resolution of 3 m near the surface which gradually increased to 22 m deeper down.

2.4 Meteorological conditions

In this section, we present a brief overview of the meteorological conditions for the study period, focussing on the characteristics that led to the surges for storms Christian and Xaver. In the last 3 months of 2013, several severe storms hit northern Europe in rapid succession (Hewson et al. 2014), causing destruction and disrupting travel (e.g. power outages in many

Fig. 1 Topography of the North Sea and buoy locations used in this study. Sea depth over 180 m is marked with *dark blue*. The *red circles* correspond to wave measurement stations and *red squares* to water-level measurement stations. The *blue dashed line* marks the zonal transect, where vertical profiles of velocity was analysed. Station BSH03 also corresponds to station ‘Elbe’



regions, serious building damages, shutting down of shipping, air and railway traffic). The storm Christian formed on 26 October 2013 over the Western Atlantic as a secondary depression of the low-pressure system Burkhard. With a translatory speed of 1200 km in 12 h, Christian was classified as ‘rapid moving low’ (DWD report 2013). In the early hours of 28 October, the storm crossed the south of the UK and moved across the southern North Sea towards Denmark. About noon, it was reported that the first hurricane force gusts (12 Bft ≥ 32.7 m/s, Haeseler and Lefebvre 2013) were measured on the German North Sea coast. The highest wind speed was observed between 13 and 14 UTC (see Fig. 2 for the FINO-1

location wind speed) over the German Bight (the weather station at Sankt Peter Ording recorded a gust of 47.7 m/s at 12:30 UTC, the maximum recorded in the meteorological network of DWD), when the centre of the storm was located off the north-west coast of Denmark with a central pressure of about 970 hPa (Haeseler and Lefebvre 2013). The high sustained winds make this storm event remarkable (see Fig. 3a). Not only the gusts but also the 10-min sustained wind speeds reached hurricane force, especially in northern Germany (Haeseler and Lefebvre 2013). Later, the storm Christian crossed the Baltic Sea area towards Scandinavia (Fig. 3b; see also Viitaka et al. 2016).

From 4 to 7 December, the storm Xaver moved from south of Iceland over the Faroe Islands to Norway and southern Sweden and across the Baltic Sea to Estonia, Latvia and Lithuania. It reached its lowest sea-level pressure on 5 December 18 UTC over Norway (about 970 hPa, see Fig. 3). It is interesting to note that over the German Bight area, the storm Xaver coincided with high tides and thus an extreme weather warning was issued to coastal areas of north-western Germany with wind gusts recorded at more than 36 m/s (Deutschländer et al. 2013). DWD reported the storm to be worse or similar to what has been experienced throughout the North Sea flood of 1962 in which 340 people lost their lives in Hamburg, stating that improvements to the sea defences since that time made them capable of withstanding the storm surge (Deutschländer et al. 2013; Lamb and Frydendahl 1991). Staneva et al. (2015) applied the General Estuarine Transport Model (GETM) for the storm Xaver and showed an exceptional sea-level increase in the German Bight. For this extreme event, sea levels were enhanced by about 40 cm through interaction with waves.

2.5 Data

The tide gauge observations are taken from the eSurge project (www.esurge.org). An overview of existing operational tide gauges in the North Sea and Baltic Sea regions are available at the Webpages of the EuroGOOS regional networks North West Shelf Operational Oceanographic System (NOOS) and Baltic Operational Oceanographic System (BOOS), respectively: www.noos.cc and www.boos.org. The water-level data used here were acquired through the NOOS server.

The wave in situ data are taken from the WMO’s Global Telecommunication System (GTS), which presents ‘communications and data management component that allows the World Weather Watch (WWW) to operate through the collection and distribution of information critical to its processes’. It is implemented and operated by the National Meteorological Services of WMO Members and International Organizations (https://www.wmo.int/pages/prog/www/TEM/GTS/index_en.html). The names and locations of the wave buoys are shown on Fig. 1. The data have been through an automated

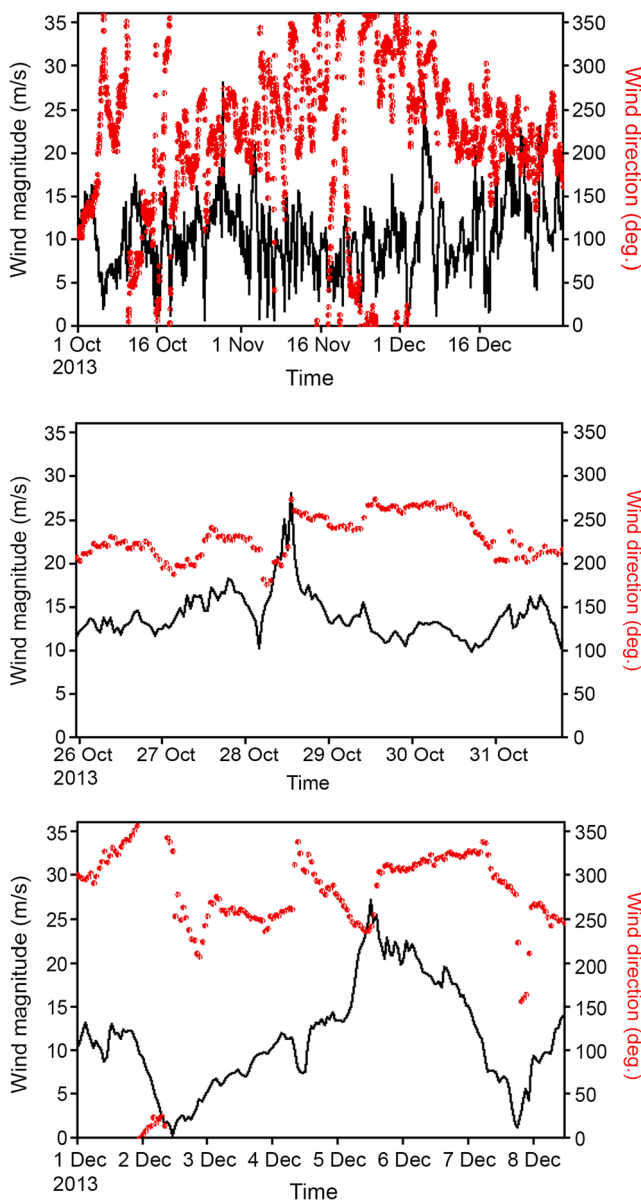


Fig. 2 Atmospheric forcing DWD 10 m wind magnitude (black line) and wind direction (red line) at FINO-1 station (see Fig. 1 for its location) during (top pattern) the whole integration period and zoomed for storm Christian (middle pattern) and storm Xaver (bottom pattern)

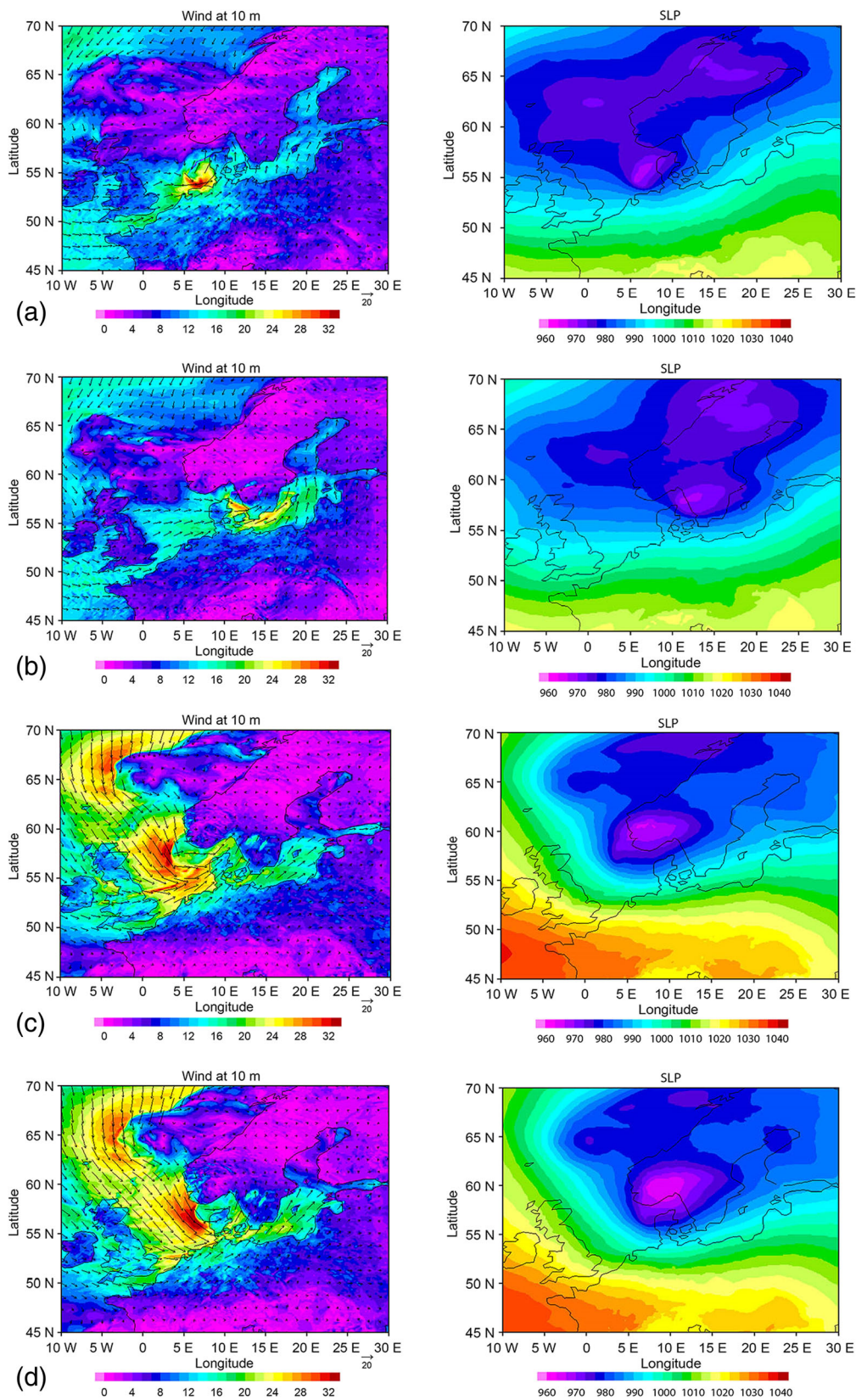


Fig. 3 Meteorological situation: *left*, 10 m wind speed (m/s; *in colour*) and wind direction (*arrows*) and *right*, sea-level pressure (dbar) during **a** storm Christian on 28 October 2013 at 15:00, **b** storm Christian on 28 October 2013 at 20:00 and storm Xaver on 05 December 2013 at **c** 11:00 and **d** 15:00

quality check upon retrieval. We have in addition visually inspected the observations to remove any gross errors.

An ADCP at FINO-1 Station (see Fig. 1 for its location) measures the current direction and velocity at 15 depth levels. All data are collected continuously on the platform and are transferred hourly to shore for further processing and presentation on the FINO Website (<http://www.bsh.de/de/Meeresdaten/Beobachtungen/MARNET-Messnetz/Stationen/fino.jsp>). The research platform FINO-1 was erected in the German Bight in 2003 as a basis for the construction and operation of an offshore wind farm. The main goal of the FINO-1 measurement project is the determination of the prevailing marine conditions (physical, hydrological, chemical and biological) in this offshore region. The type of ADCP used (Nortek Acoustic Wave and Current Meter (AWAC)) is designed to measure current profiles and wave parameters. Unfortunately, in the period of the storm Xaver, FINO-1 was the only platform providing ADCP measurements over our study area. No additional quality control has been done for the observational data.

3 Wave effects in the ocean model

The NEMO ocean model has been modified to take into account the following wave effects: (1) The Stokes-Coriolis

forcing (Hasselmann 1970), (2) Sea-state-dependent momentum flux (Janssen 1989; Janssen 2012) and (3) Sea-state-dependent energy flux (Craig and Banner 1994; Breivik et al. 2015). Note that in this study, we used a wave-induced forced mode into the ocean model NEMO (one-way coupling). All technical details can be found in Janssen et al. (2013) as well as in ECMWF (2014). In this section, we will only briefly describe the wave-hydrodynamic interaction mechanisms that have been implemented in NEMO.

3.1 Stokes-Coriolis forcing

Fluid particle trajectories in water waves do not form perfectly closed orbits because of the different speed of wave crests and wave troughs. This sets up a second-order effect, which leads to a discrepancy between the average Lagrangian flow velocity of a fluid parcel and the Eulerian flow velocity known as the Stokes drift (Stokes 1847). As is the case for the wind-induced currents, the Stokes drift also interacts with the Earth’s rotation. This adds an additional veering to the ocean currents known as the Stokes-Coriolis force (Hasselmann 1970):

$$\frac{D\mathbf{u}}{Dt} = -\frac{1}{\rho}\nabla p + (\mathbf{u} + \mathbf{v}_s) \times f \hat{\mathbf{z}} + \frac{1}{\rho} \frac{\partial \tau}{\partial z} \tag{3}$$

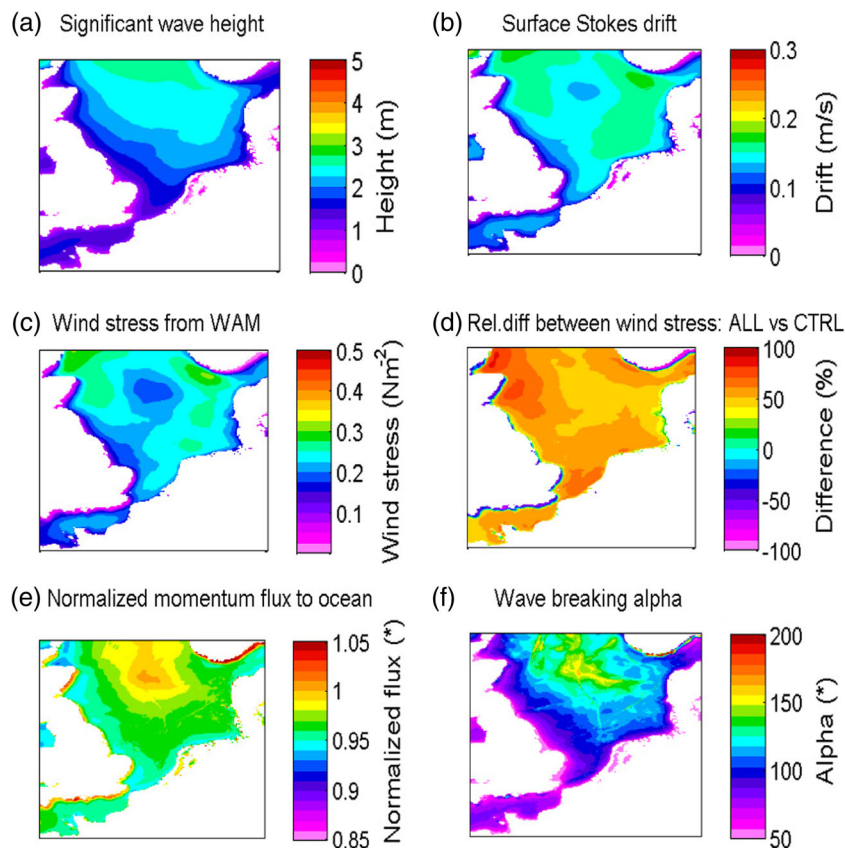


Fig. 4 Wave processes averaged for the 3-month period (01 October Institute for Coastal Research 2013–31 December 2013)

Where \mathbf{v}_s is the Stokes drift vector, p is the pressure, $\boldsymbol{\tau}$ is the surface stress and $\hat{\mathbf{z}}$ is the upward unit vector. Because calculating the full vertical profile is costly, the Stokes drift velocity profile is calculated with an approximation given by Breivik et al. (2014). Recently, Breivik et al. (2016) suggested a better approximation of the Stokes-Coriolis forcing.

The mean Stokes drift circulation over the 3-month integration period is relatively small (less than 0.2 m/s, Fig. 4b) even in the northern part of the area where the mean significant wave height exceeds 2 m (Fig. 4a). However, during the storm Christian, in the southern North Sea the 2-day averaged Stokes velocity has a maximum of about 0.4 m/s (Fig. 5b) for the German Bight area, where the significant wave height exceeded 3.5 m (Fig. 5a). Good correlation between the horizontal patterns of significant wave height (H_s) and Stokes drift velocity is observed for the Storm Christian. In the time of storm Xaver, in the area near the Danish straits the H_s exceeds 10 m (Fig. 6a) and the Stokes drift is about 0.8 m/s (Fig. 6b), i.e. of the same order as the wind-induced Eulerian surface current speed for this area.

3.2 Sea-state-dependent momentum flux

The momentum flux going into NEMO from WAM depends on (1) the wave-modified drag coefficient, which changes the air-side stress and (2) on the ocean-side stress, which depends on the balance between wave growth and dissipation.

In the presence of growing waves, the roughness felt by the airflow also changes with time because momentum is extracted from the wind to generate waves. Let us denote this flux of momentum by τ_{in} . Let us also define the air-side stress (τ_a) and air-side friction velocity (u_*). The latter are related as:

$$u_*^2 = \frac{\tau_a}{\rho_a}, \quad (4)$$

where ρ_a is the surface air density. Charnock (1955) related the roughness of the sea surface to the friction velocity:

$$z_0 = \alpha_{CH} \frac{u_*^2}{g}, \quad (5)$$

where α_{CH} is known as the Charnock constant. Janssen (1989) assumed that α_{CH} is not a constant, but instead that it varies with the sea state:

$$\alpha_{CH} = \frac{\hat{\alpha}_{CH}}{\sqrt{1 - \tau_{in}/\tau_a}}, \quad (6)$$

where $\hat{\alpha}_{CH} = 0.006$. The wave-induced stress is related to the wind input to the wave field as:

$$\tau_{in} = \rho_w g \int_0^{2\pi} \int_0^\infty \frac{\mathbf{k}}{\omega} S_{in} d\omega d\theta, \quad (7)$$

where ρ_w is water density and ω is the wave angular frequency. The wave-modified drag coefficient takes the form

$$C_D = \frac{\kappa^2}{\log^2(10/z_0)}, \quad (8)$$

where $\kappa = 0.4$ is von Karman's constant. Note that the drag coefficient as defined here is applied to the 10-m neutral wind speed. This drag coefficient is computed by WAM. The average wind stress from WAM is shown in Figs. 4c, 5 and 6c for the whole integration period, for the storm Christian and for storm Xaver, respectively. This wind stress is calculated by using the drag coefficient obtained with Eq. (8). This is the stress which goes into NEMO and is then modified by the normalised ocean-side stress (described below). The relative difference between the wind stress calculated by taking into account waves (Eq. 8) and that from the standard bulk formulae used in NEMO is shown in Figs. 4, 5 and 6d. The presence of waves greatly affects the wind stress (Figs. 4d, 5 and 6d). For the 3-month period (Fig. 4d), the relative difference is calculated on the basis of cumulative wind stress, while for Figs. 5d and 6d, the relative difference is calculated for wind stress cumulated over storms Christian and Xaver, respectively. For both storms, the stress increases by 100 % and more. For Christian, the largest increase is in the coastal waters of Germany and the Netherlands (Fig. 5d), while for Xaver, the offshore areas exhibit the largest increase in wind stress, if waves are accounted for (Fig. 5d).

However, not all of this stress is directly available to the ocean. As waves grow, they absorb momentum from the atmosphere and the ocean current therefore feels less stress. However, as waves mature and break, they release momentum to the ocean. The total balance on the water side thus becomes

$$\tau_{oc} = \tau_a - \tau_{in} - \tau_{db}, \quad (9)$$

where τ_{db} is the momentum injected by breaking waves (negative) and can be estimated from the wave dissipation source term S_{wc} in Eq. (2). Only if the input of momentum by wind is balanced by the release of momentum through breaking (fully developed sea) will the ocean-side stress balance the atmospheric stress. More details on how τ_{in} and τ_{db} are computed and the technical implementation can be found in the ECWAM documentation part VII, Sect. 6.7 and also in ECMWF (2014; <https://software.ecmwf.int/wiki/display/IFS/CY40R1+Official+IFS+Documentation>). In our current implementation of WAM, the ocean-side stress is output as a normalised quantity and is applied as a correcting factor to the air-side stress in NEMO (Breivik et al. 2015).

The normalised momentum flux

$$\tilde{\tau} = \frac{\tau_{oc}}{\tau_a} \quad (10)$$

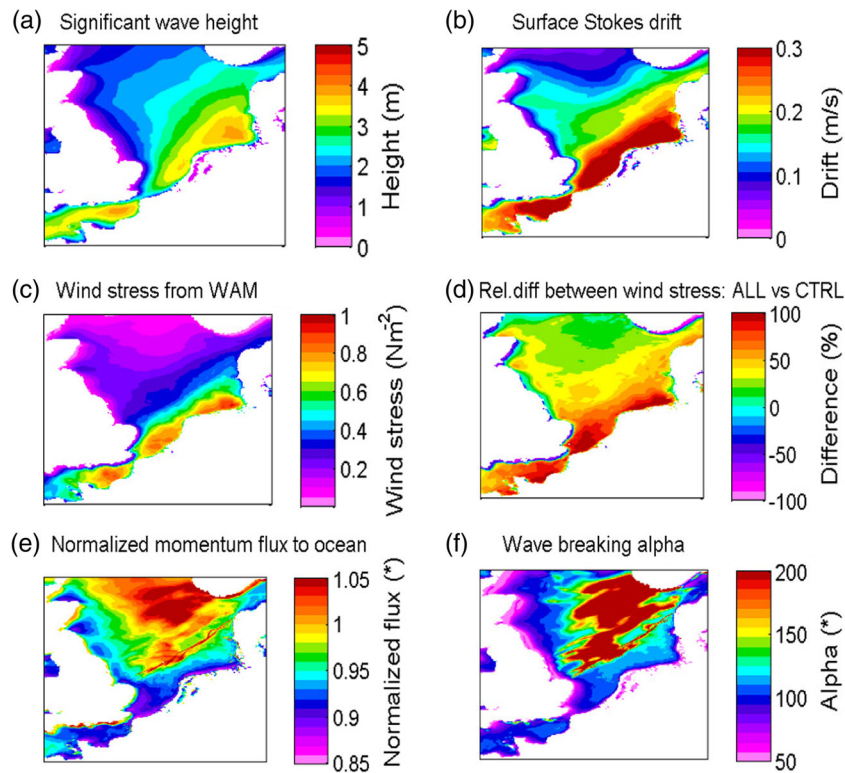


Fig. 5 Wave processes during the storm Christian averaged from 28 October 2013 at 00:00 to 29 October 2013 at 23:00

processed in NEMO for the 3-month integration period (Fig. 4e) and in the periods of storms Christian (Fig. 5e) and Xaver (Fig. 6e) are shown. Note that in the areas of active wave growth, the normalised momentum flux is less than unity (see,

for example the patterns for Christian (Fig. 5e) in the south-eastern North Sea. Including waves in the momentum flux parameterisation leads to an ocean-side stress, which is less than the atmospheric stress in growing seas. On the other hand, in the

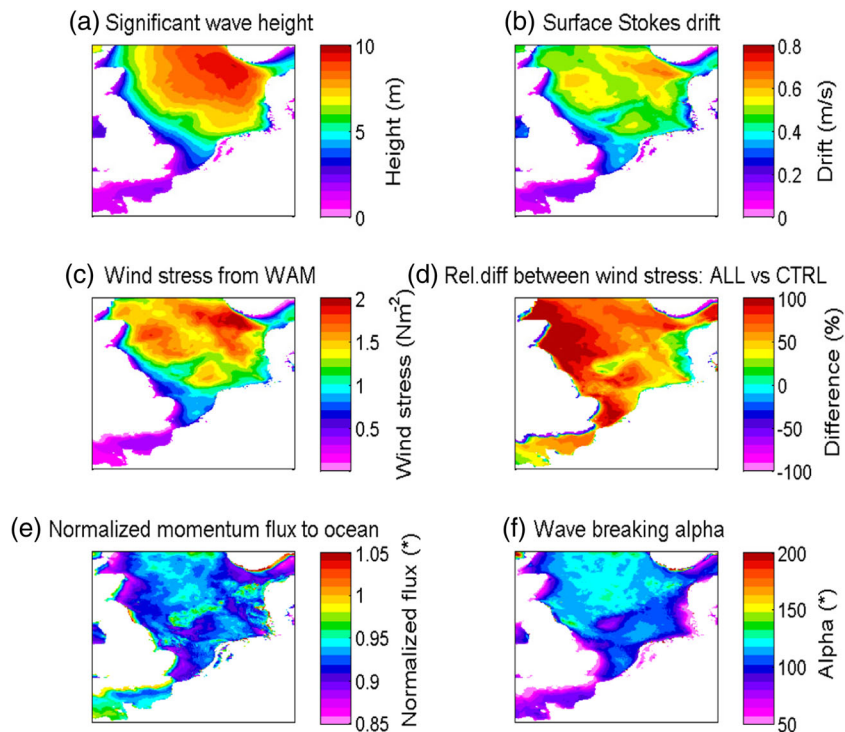


Fig. 6 Wave processes during the storm during Xaver averaged from 05 December 2013 at 00:00 to 06 December 2013 at 23:00

Table 1 Summary of model experiments

Experiment	Description of experiment
CTRL	Control simulation, without wave model
ALLWAVE	All three wave processes included
TAUOC	Sea-state-dependent momentum flux included only
TKE	Sea-state-dependent energy flux included only
STCOR	Stokes-Coriolis forcing included only

areas in which waves are decaying and therefore losing momentum, the normalised momentum flux exceeds unity (see, for example the northern-western area for storm Christian, Fig. 5e). During the storm Xaver (Fig. 6e), the ocean-side stress differed from the atmospheric stress by about 20 %. Over the whole integration period (Fig. 4e), the differences between the atmospheric and the wave-induced stress are much pronounced

in the shallow North Sea areas whereas in the open sea the decrease of the stress caused by waves is less than 5 %.

3.3 Sea-state-dependent energy flux

In NEMO, the wave-induced turbulent kinetic energy (TKE) flux introduced at the sea surface depends on the wave energy factor α (Craig and Banner 1994) and is set to a constant value regardless of sea state. Craig and Banner (1994) argued that the turbulent kinetic energy flux is relatively insensitive to the sea state and is well approximated by αu_{w*}^3 (u_{w*} is water friction velocity) and $\alpha = 100$ was thought to be representative of a mid-range of sea states between young wind seas and fully developed situations. From the full spectral wave model, it is possible to estimate directly both the energy and energy flux from the wave-breaking source terms (Breivik et al. 2015, see also ECMWF 2014). The horizontal patterns of the wave energy factor α over

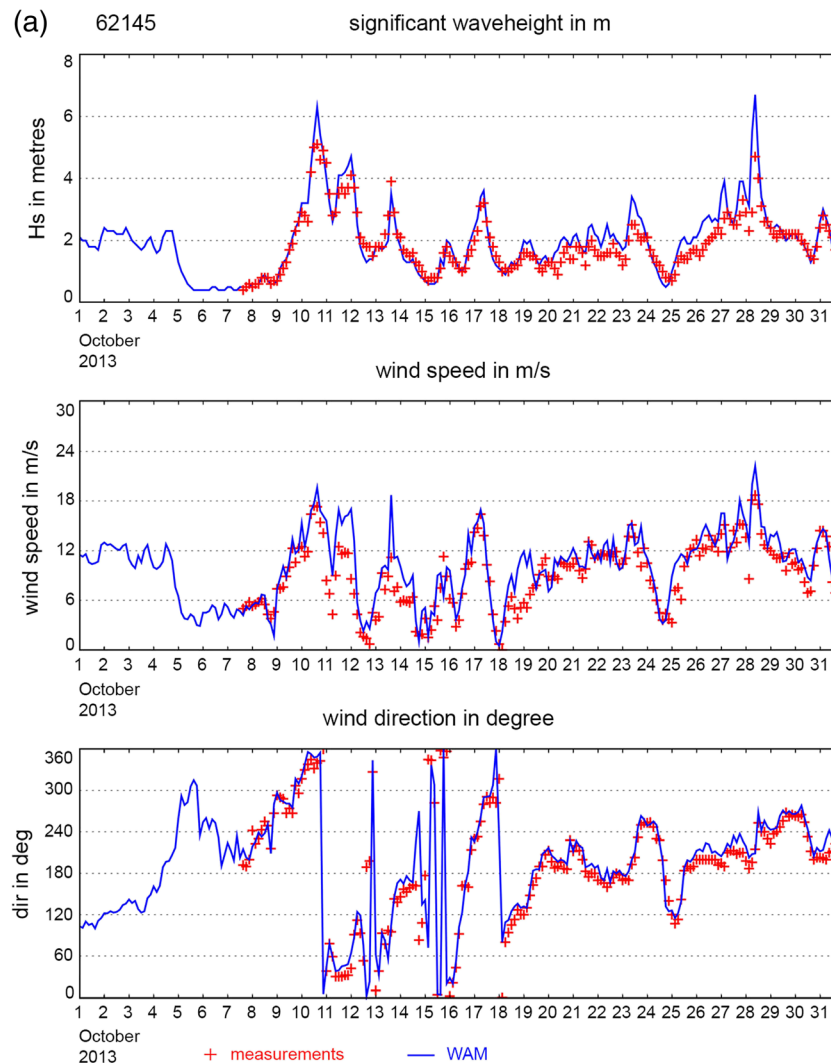


Fig. 7 Top, significant wave height (H_s ; m); middle, wind magnitude (m/s) and bottom, wind direction validations at station 62145 (see Fig. 4 for its location) for **a** October 2013 and **b** 1–20 December 2013. Red symbols—observations; blue line—model simulations

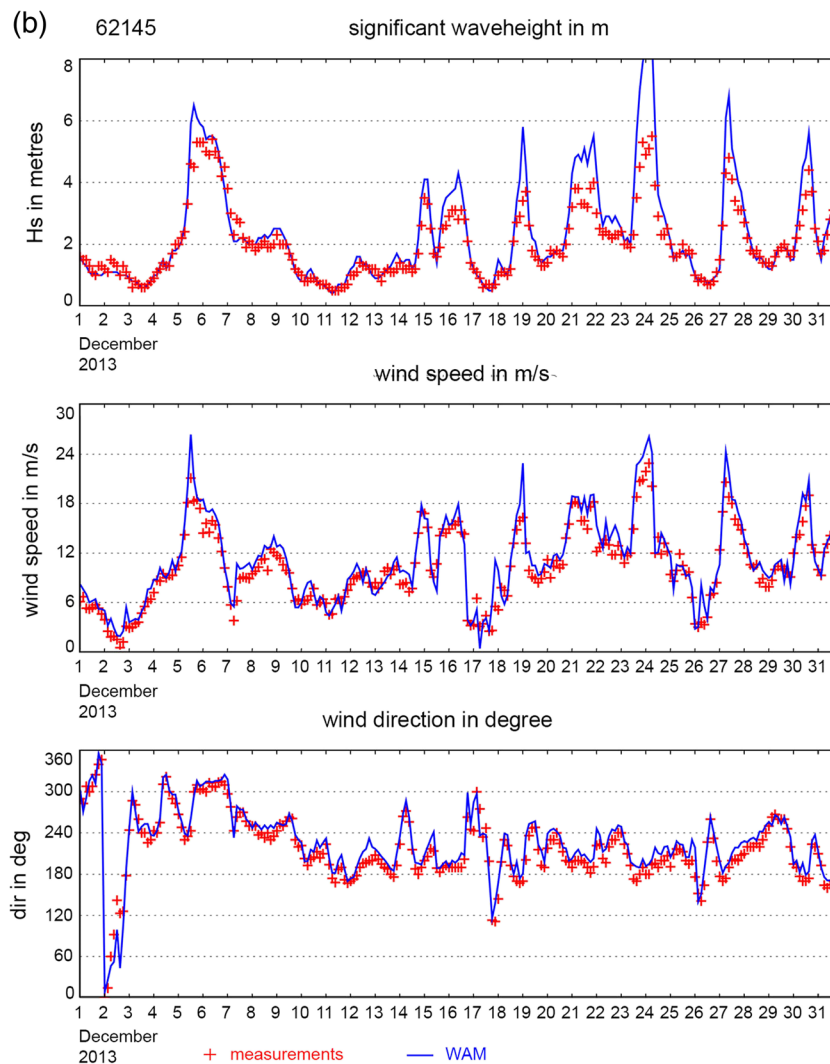


Fig. 7 (continued)

the whole integration period, the storms Christian and Xaver are shown in Figs. 4, 5 and 6f, respectively. Depending on the dissipation intensity and the wind variability, the wave factor α varies between 20 and 400. It is important to stress that for the control experiment (without wave model input), the standard value of 100 is used while for the experiment in which the state-dependent energy flux is included, the values are estimated from the wave model as described in this section.

In NEMO, the boundary condition of the turbulent length scale z_0 on the water side of the air-sea interface follows the Charnock relation:

$$z_0 = \frac{\beta u_{w*}^2}{g} \tag{12}$$

where u_{w*} is the water-side friction velocity, β is the Charnock constant and g is the acceleration caused by gravity. The

turbulent length scale in the water is orders of magnitudes larger than its air-side counterpart.

In the default version of NEMO, the Charnock constant has a value of 2×10^5 , which was the value found by Stacey (1999) by minimising the errors between measured and modelled currents. Moreover, Stacey (1999) found that z_0 is in the order of significant wave height. Other workers (Craig and Banner 1994; Terray et al. 1996; Drennan et al. 1996) have similarly found it to be of the order of the wave amplitude up to the significant wave height. In this study, we also make the assumption that z_0 scales with significant wave height, and therefore in NEMO, we substitute the H_s for z_0 .

3.4 Model experiments

For the control experiment (CTRL), NEMO is run without a wave model and the energy flux from breaking waves is parameterised according to Craig and Banner

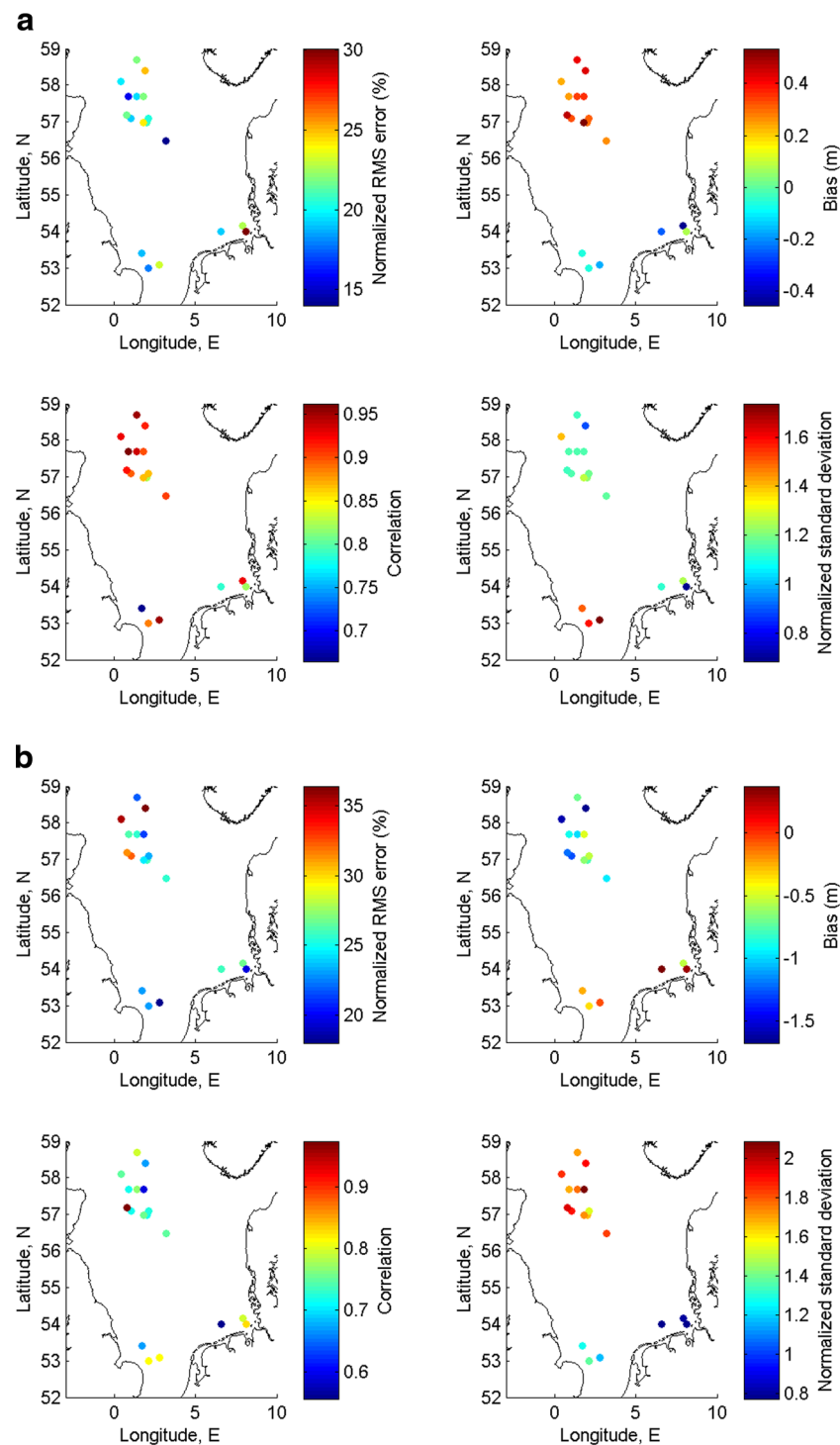


Fig. 8 Statistics between the model simulations and observations for the significant wave height *Top left*, normalised RMS error (%); *top right*, bias (m); *bottom left*, correlation and *bottom right*, normalised standard

deviation for **a** storm Christian at averaged for 28–29 October 2013 and **b** storm Xaver at averaged for 5–6 December 2013, **c** averaged over the whole period and **d** averaged for November 2013

(1994) and Mellor (2004) with $\alpha = 100$ and the water-side Charnock constant $\beta = 1400$. This control experiment is compared with wave-forced model simulations in which NEMO sees the stresses, turbulent fluxes and

Stokes drift (described in Sect. 3.3) calculated by WAM. In these experiments, either all three wave effects (experiment ALL) are activated or the individual mechanisms are switched on separately to assess the impact

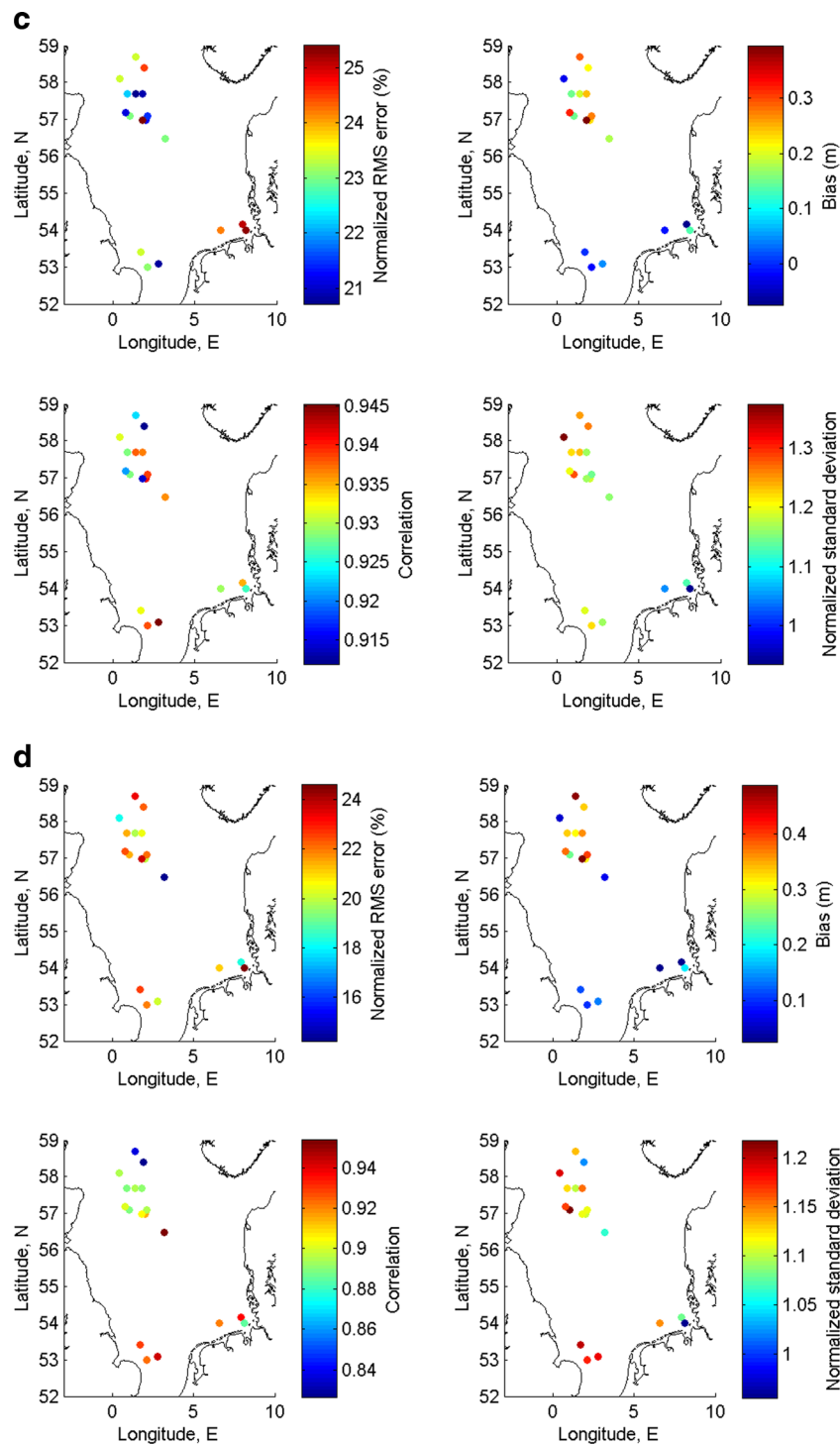


Fig. 8 (continued)

of each process. The three additional experiments in which the individual processes considered are (i) sea-state-dependent momentum flux (experiment TAUOC), (ii) sea-state-dependent energy flux (experiment TKE) and (iii) Stokes-Coriolis forcing (experiment STCOR). These experiments are summarised in Table 1.

4 Model performance during extremes

4.1 Wave model performance

In this section, we quantify the performance of the wave model during the two storms Christian and Xaver using a series of

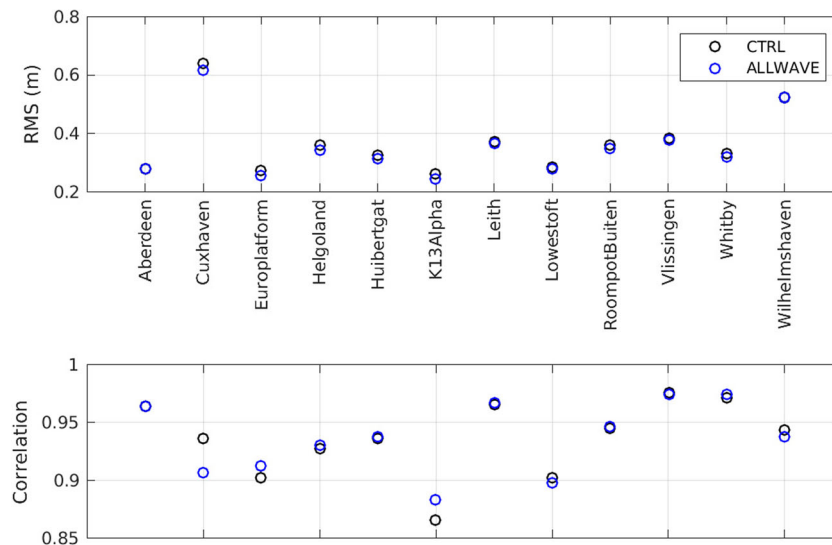


Fig. 9 Statistics of simulated SLA with respect to the tide gauges data during the integration period (01 October 2013–30 December 2013), *top*, RMS (m) and *bottom*, correlation during the whole integration period

different statistical parameters computed for these extremes and compare with statistics obtained for the whole integration period as well as for November, which is a period characterised by relatively calm wind conditions (see Fig. 2). The locations and the water depth (illustrated with colours) of the wave in situ data, where we performed the statistical analyses, are shown in Fig. 1. Wind magnitude and direction, as well as WAM-simulated H_s are in good agreement with the measured values, and as an example, we present a time series for station 62145 in October (storm Christian, Fig. 7a) and December (storm Xaver, Fig. 7b). The significant wave height for this station shows a correlation coefficient of 0.95 and a root mean square error (RMSE) of 0.37 m. The bias between model predictions and observations is 0.04 m. In the period of the two extremes, the measured H_s was above 4.5 and 5.4 m, respectively. For Xaver, the wave model overestimated the H_s (by

about 0.8 m, see Fig. 7b). For the mean wave period at the same station, the correlation is 0.86 and the RMSE is 0.66 s. The ‘peakiness’ of the DWD winds is probably due to the time discretisation caused by obtaining hourly fields. For all available North Sea stations, the computed statistical values, such as normalised RMSE, bias, correlation and normalised standard deviation show quite good homogeneity for all four periods (Fig. 8). The mean of the observations at each location was used to estimate the normalised standard deviation. The correlation coefficients between the WAM simulations and measurements were always high—above 0.9 for all stations and the normalised RMS error was relatively low. Storm Xaver builds the highest waves in the North Sea, exceeding 14 m near the Danish Straits (Fig. 6a), while the maximum H_s for Christian occurred in the German Bight area (Fig. 5a). The waves are reproduced in our model system with good

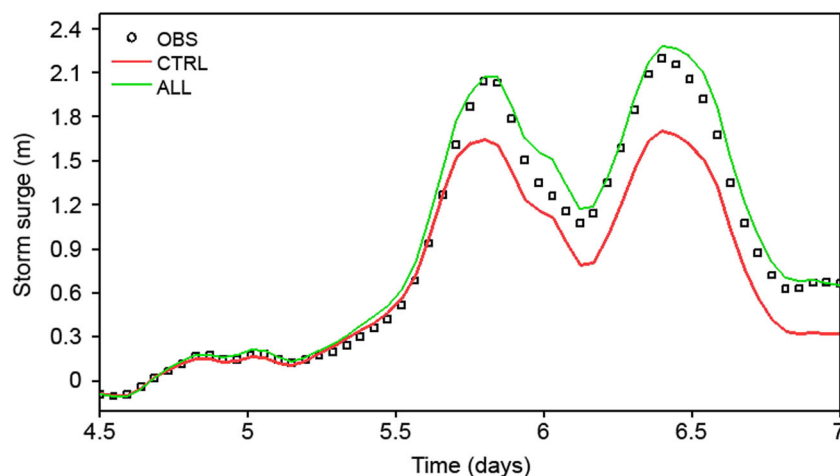


Fig. 10 Observed (black squares) against computed storm surges for the circulation model only (CTRL run—red line) and the coupled wave-circulation model (ALL run—green line) during storm Xaver at station Helgoland. The x -axis corresponds to the time in days from 01 December 2013

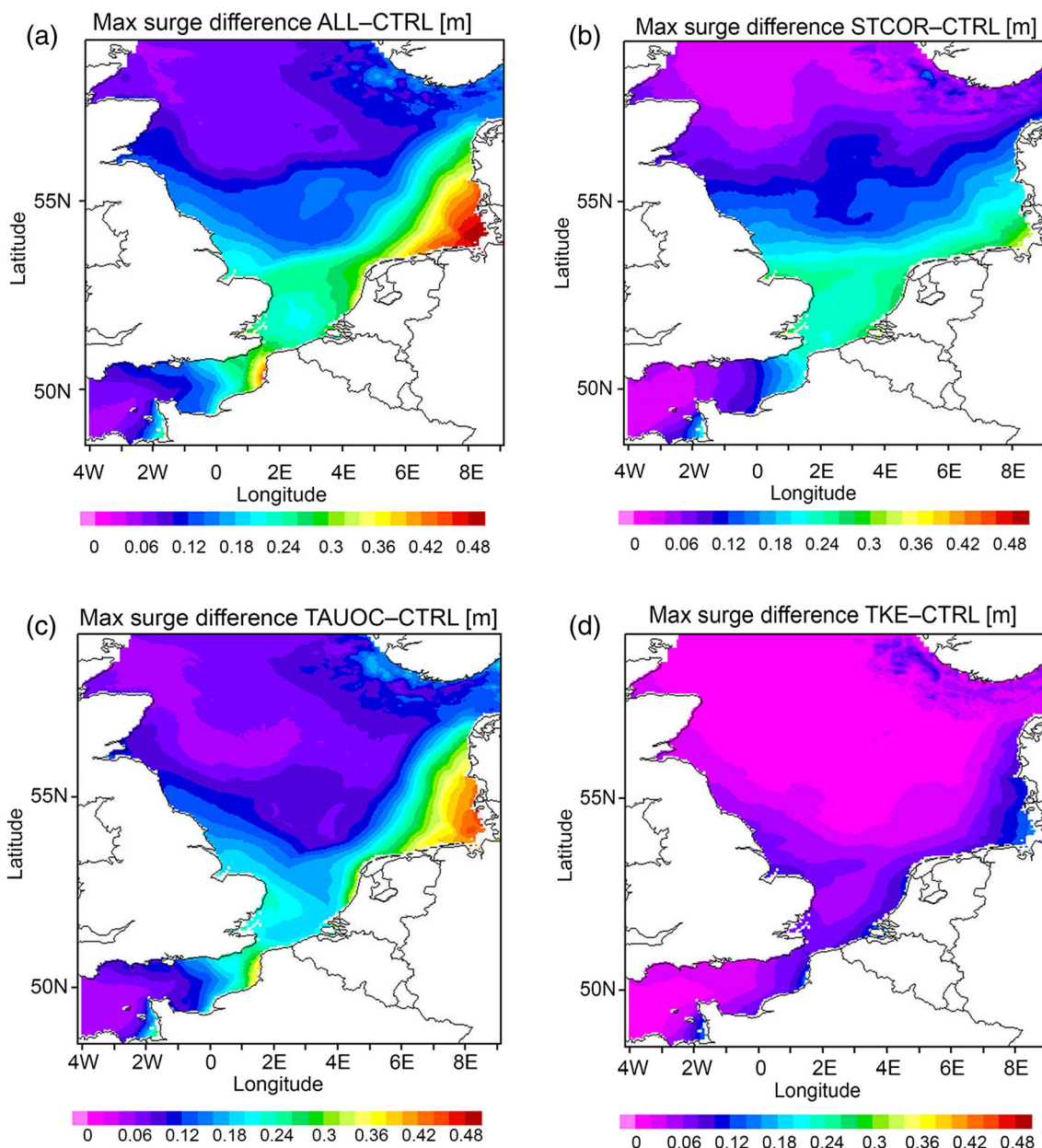


Fig. 11 Maximum surge difference (m) during storm Christian (26–29 October) between **a** ALL and CTRL runs, **b** STCOR and CTRL runs, **c** TAUOC and CTRL runs and **d** TKE and CTRL runs

accuracy (the bias for Christian is less than 0.1 m, Fig. 8a). From the statistical analyses shown in Fig. 8, it can be concluded that the wave model results for the whole North Sea area are in very good agreement with measurements not only for the calm conditions (Fig. 8d) but most importantly, for storms Christian and Xaver—both behaving rather differently (Fig. 8a, b). For storm Xaver, the bias in the north-western area is higher, which might be caused by inaccurate boundary conditions. During both storms, the normalised RMSE for the German Bight is higher than for the rest of the North Sea (Fig. 8). This can be caused by the relatively coarse spatial resolution and consequently smoother model bathymetry in the shallow coastal waters.

4.2 Sea-level variability and wave-induced forcing

In Fig. 9, a validation of the simulated sea level against observational data is presented. Including wave-current interaction processes improved the RMSE and the correlation coefficient between the tide gauge data and the simulated sea level. For almost all stations, the correlation coefficient for the whole integration period is above 0.9. For the 3-month period, the bias between observations and model data lies in the range of 0.2–0.3 m, except for the near coastal station Cuxhaven, which may again be the result of the relatively coarse resolution of the model.

From the simulations and model observations, storm surges were computed by subtracting the ocean tide computed with the

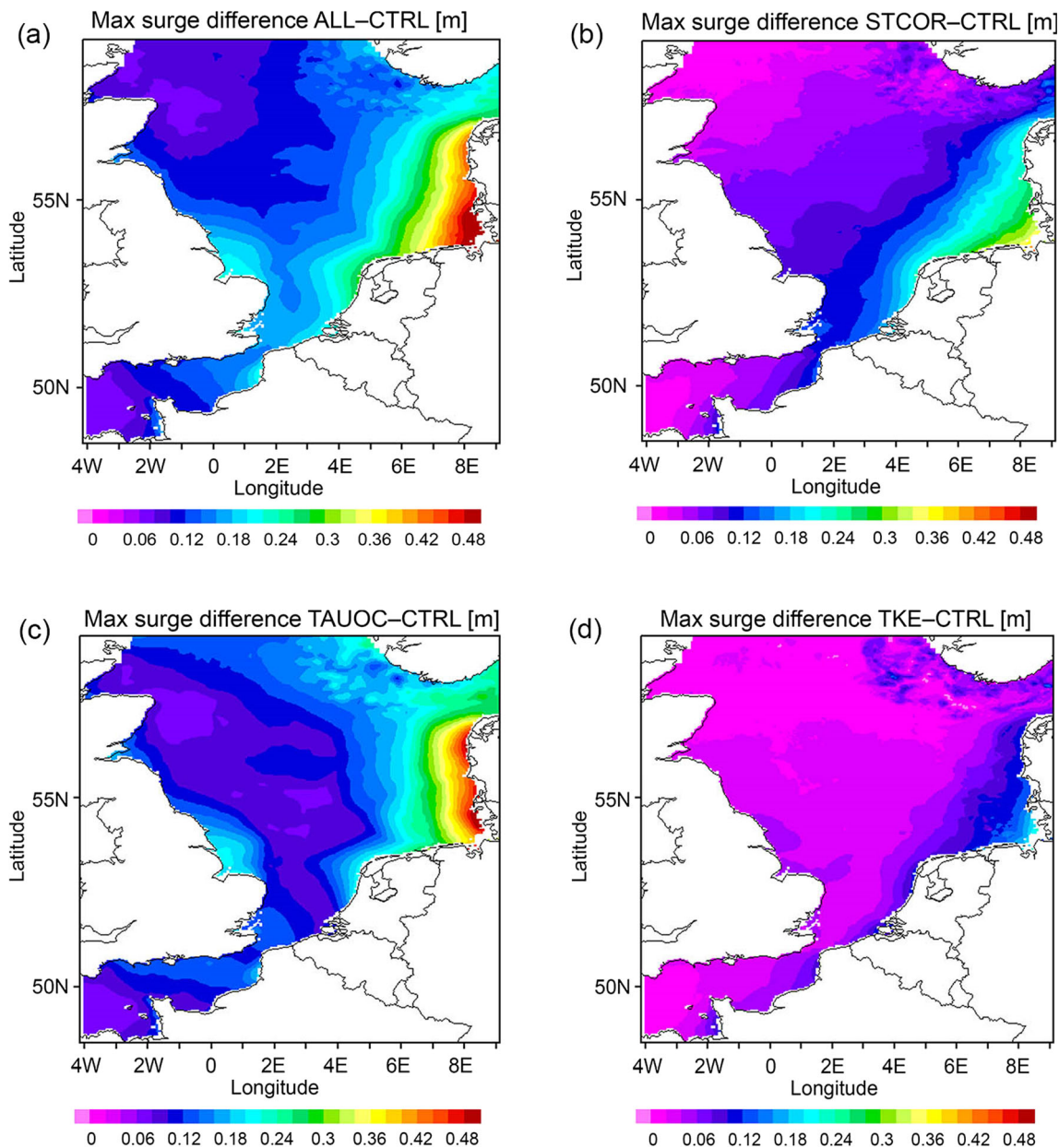


Fig. 12 Same as Fig. 11 but for storm Xaver (05–06 December 2013)

T_TIDE software (Pawlowicz 2002) from the tide gauge readings to obtain the storm surge height at the tide gauge. At the time of the storm Xaver, for the German Bight area, the surge height reached values of about 2.5 m. Fenoglio-Marc et al. (2015) described the first maximum as a wind-induced one. They demonstrated also that for the Aberdeen and Lowestoft stations in the UK (located 550 km apart), only one maximum was observed by the tide gauges, suggesting a Kelvin wave propagating anticlockwise along the coasts of the North Sea, reaching the eastern coast about 10 h later than in Lowestoft (easternmost UK coast), causing the second storm surge maximum observed at all the German stations. These two storm surge maxima are reproduced by both the NEMO model only (CTRL

run) and by the wave-forced NEMO model (ALL run, see Fig. 10). The two maxima for the Helgoland stations are underestimated by the stand-alone circulation model, especially over the extremes, where the surge difference between observations and model simulations is about 30 cm for the first peak and more than 40 cm for the second peak. The sea-state-dependent integration (ALL) leads to a persistent increase of the surge after the occurrence of the first maximum (with slight overestimation after the second peak) and remains substantial in the following 2 days.

In order to assess the relative impact of the three wave-induced processes, we show the horizontal patterns of the maximum difference between the four-wave-forced

simulations (ALL, STCOR, TAUOC and TKE) and the CTRL run (no explicit wave effects) found during the extent of the two storm events (Christian and Xaver) in Figs. 11 and 12, respectively. It is important to mention here that the ALL run is not a linear combination between the three runs considering the wave-induced processes separately (TKE, STCOR, TAUOC runs) but rather we aim to identify which of them are dominant for the changes in the water level over the extreme events.

The patterns show that the differences between the wave-forced and circulation model only are more pronounced along low-lying coastal areas along the South-eastern North Sea coasts. The maximum difference between ALL and CTRL runs is about 48 cm and is simulated for storm Xaver along the German Bight coastal region (Fig. 12a). Over storm Christian, it is about 44 cm and is concentrated along the Elbe river area (Fig. 11a). A similar effect of coupling between wave and circulation models has been shown by Staneva et al. (2015) albeit with a much higher resolution (1 km) coastal model for the German Bight area only. Comparing the different patterns in Figs. 11 and 12, we can conclude that it is mainly caused by the sea-state-dependent momentum flux (Figs. 11c and 12c) and, to a lesser extent, by the Stokes-Coriolis forcing (Figs. 11b and 12b). For storm Christian, the wave-dependent momentum flux contributes by increasing the sea level along the southern North Sea and towards the Elbe river area. For storm Xaver, the increase is strengthened towards the North-Frisian Wadden Sea coast. The computed maximum surge differences are higher during Xaver than those obtained during Christian. The horizontal distribution of the patterns of Figs. 11 and 12 are consistent with the meteorological situation (Fig. 2) and the horizontal distribution of the H_s (Figs. 5 and 6) in the period of the two storms. The Stokes drift has a southward component (Fig. 5) for both extremes, increasing the water level, which is higher in the south-eastern North Sea along the Dutch and German coastal areas (about 20–30 cm, see Figs. 11b and 13b). Considering the third component, the differences for the changes in the TKE are much smaller (Fig. 12d). The effects of wave-induced forcing over the two storms are also observed in the open North Sea (maximum surge differences are about 15 cm (Figs. 11a and 12a) and are caused by the Stokes-Coriolis forcing (Figs. 12b and 13b) and sea-state-dependent momentum flux (Figs. 11d and 12d). The impact of wave-induced turbulence is mostly narrowly confined along the south-eastern coastline for both Christian and Xaver (Figs. 11d and 12d, respectively). The increase in the maximum differences towards the shallow southern part of the area can be explained by the modified surface stress. Even though the H_s was much higher in the north-eastern area closer to the Danish straits (see Fig. 5), the water there is much deeper and thus the differences in sea level are relatively small. The differences between the spatial patterns of the two extremes are also

caused by the different tracks, intensity and duration of the storms (Figs. 2 and 3).

4.3 The impact of wind waves on currents

Besides examining the sea-surface elevation, we consider also the time variation of the currents. Station FINO-1 (see Fig. 1 for its location) has ADCP observations (described in Sect. 2) (Figs. 13 and 14). The time series that we analysed are the magnitude of the circulation for the depths of 2, 6 and 14 m, respectively. The increase in current velocity at the storm is explained by a significant contribution of the wind-induced stress in the German Bight area. The time variability of the currents from the ALL run is closer to the ones obtained by the

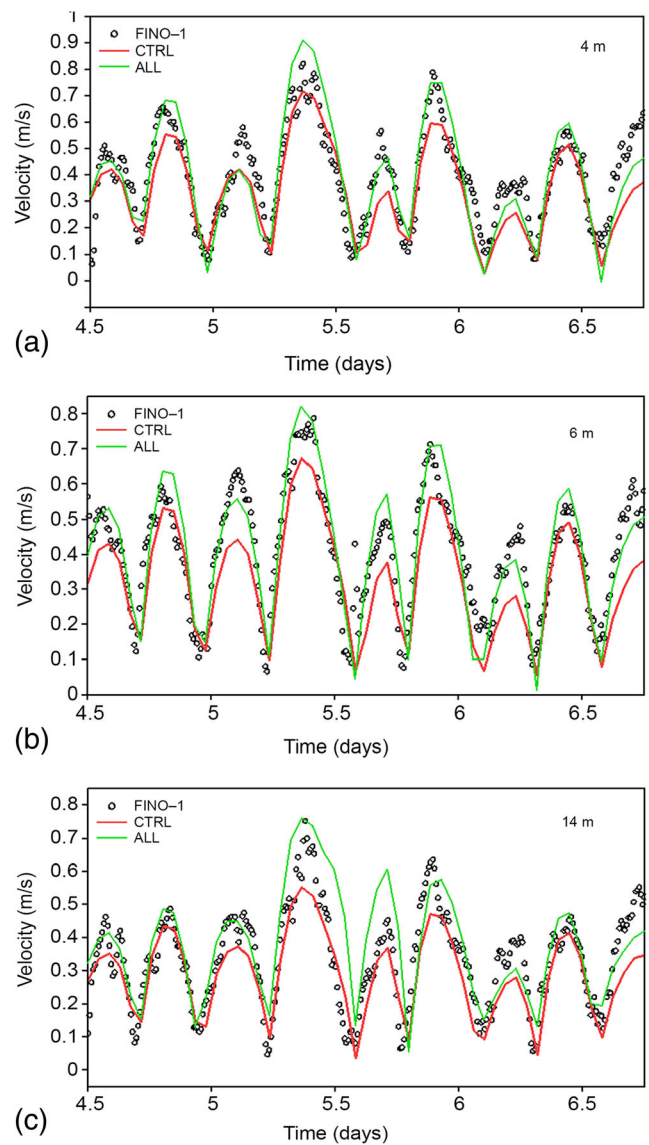


Fig. 13 Time series of velocity (m/s) from ADCP (black circles), CTRL (red line) model and ALL (green line) model runs at different levels at **a** 4, **b** 6 and **c** 14 m. The x-axis corresponds to the time in days from 01 December 2013

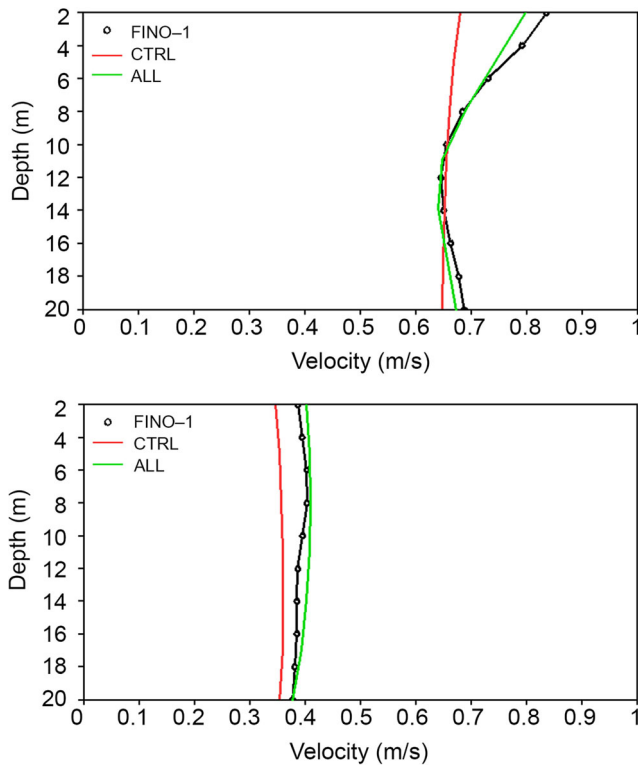


Fig. 14 Vertical profiles of velocity magnitude (m/s) from ADCP (black dots), CTRL (red line) model and ALL (green line) model runs at different levels on 05 December 2015 at 09:00 and 05 December 2014 at 14:00

ADCP data, especially in the periods of the peaks. For Xaver, the differences of the velocity between ALL and CTRL runs are more than 0.15 m/s at all depths. The magnitude of the

velocity peaks for the deeper levels is lower for both observations and simulations. The differences between the ALL and CTRL currents speed decrease with the depth, suggesting that the wave energy dissipates in the upper layers. When the velocity is minimal, both the CTRL and ALL runs show similar results, which are also very close to the one of the ADCP measurements (with differences of less than 0.05 m/s).

The vertical profiles of the velocity at 5 December 2013 for 09:00 and 14:00 UTC (Fig. 14) simulated by the ALL experiment (green line) is also closer to the one of the ADCP measurements (black line) than the velocity of the CTRL run only (red line). The minimum in the velocity profile at 09:00 observed at FINO-1 has been well reproduced by the ALL experiment and is caused by the inclusion of the Stokes-Coriolis forcing, whereas the CTRL run profile is very homogenous in depth (Fig. 14a). Similarly, for 14:00 UTC, the velocity profile of the ALL run is closer to the observational data, whereas the CTRL run underestimates the magnitude of the current at all vertical levels.

The intensification of the along-shore velocity (Fig. 15) during Xaver caused by the wave-induced processes is clearly seen in the zonal velocity section through the FINO-1 station. A similar effect has previously been documented by Grashorn et al. (2015). The increase in zonal velocity is particularly strong in the eastern, shallower, part where intense longshore currents are generated by wind waves. A maximum velocity of about 0.9 m/s is found at the sea surface in both the TAUOC and ALL runs at 6.3° E, while for the CTRL run, the maximum zonal velocity is 0.65 m/s. The increase of the surface zonal velocity for the ALL run in the eastern part is caused by the wave-induced stress, and the velocity changes in depth can

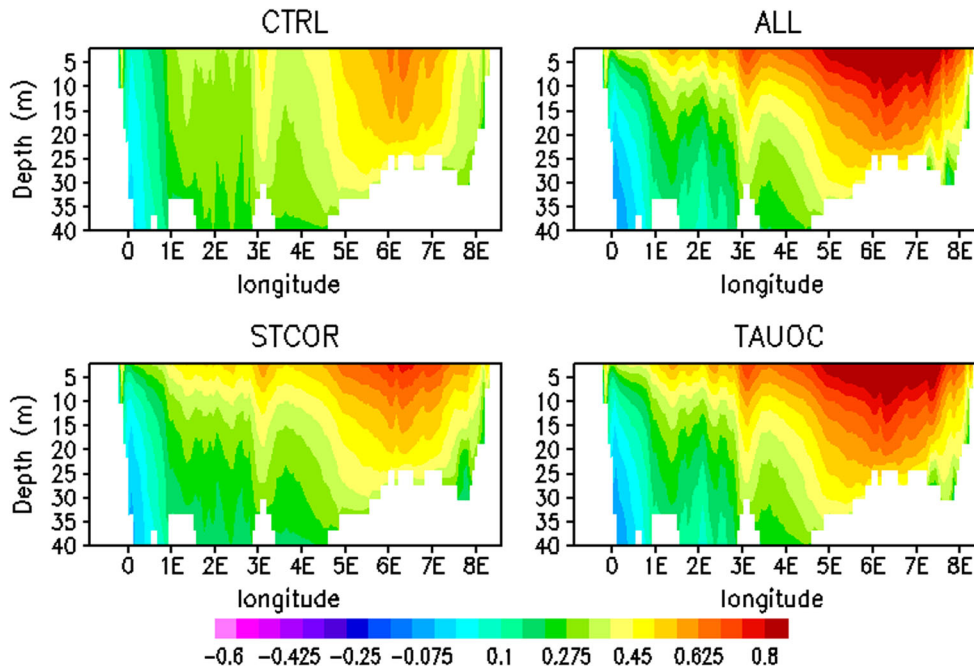


Fig. 15 Zonal velocity (m/s) through FINO-1 Station during storm Xaver (on 05 December 2013 at 09:00) for the different experiments

be explained by the combined role of the Stokes drift forcing and the wave-induced turbulence.

5 Conclusions

This study demonstrates the model performance and the contribution of the wind-wave-induced mechanisms during the storms Christian and Xaver in 2013. The 3D circulation model NEMO has been implemented by including three wave effects on a model domain covering the North Sea, namely the sea-state-dependent water-side stress, the energy flux from breaking waves and the Stokes-Coriolis force. Comparing the model simulations from the circulation model alone to the ones including different wave-interaction mechanisms (ALL, TKE, TAUOC, STCOR), we demonstrated that the impact of the wave effects is particularly noticeable for the southern shallow North Sea regions.

The predicted values of the NEMO-only simulation and the wave-forced NEMO integrations were compared against measurements at several stations located in the North Sea. The comparison with wave measurements indicated that the wave model performs quite satisfactorily not only for calm conditions but importantly also in storm conditions. The quality of the wind fields is obviously of primary importance, and we found the DWD high-resolution wind fields to be in good agreement with observations.

We found improved skill in the predicted sea level and circulation during storm conditions when using a wave-forced circulation model system. In the periods of storm events, the ocean stress was significantly enhanced by the wind-wave interaction leading to an increase in the estimated storm surge (compared with the ocean-only integration) to values closer to the observed water level. The numerical experiment with the wave-forced NEMO model yielded an increase of 48 cm in and surge level in the south-eastern shallow North Sea and along the North-Frisian Wadden Sea coast for the Xaver event, while for Christian the maximum difference was about 40 cm along the Elbe estuary.

Another novel aspect of the present work is the demonstration of the impact of wind waves on the estuarine circulation. The impact of wind waves estimated by the difference between CTRL and ALL experiments reveals the interplay between tides and waves resulting in a change of the velocity distribution. We also demonstrate that the currents induced by including wave forcing mechanisms come closer to ADCP observations than the ocean-only integration over the upper 20 m. By including wave-induced mixing, the representation of the circulation is also significantly improved.

Accounting for wind-wave effects in the three-dimensional hydrodynamical model improves predictions of water level

and currents in the shallow coastal waters. We have demonstrated here that wave effects are very important in the shallow North Sea areas during storms, and that the WAM and NEMO models can be run in sequence to form an efficient forecast system for storm surges and waves.

Acknowledgements This work was supported by CMEMS COPERNICUS Grant WAVE2NEMO and the FP7 project MyWave (grant no. 284455). ØB is grateful for the additional support of the Norwegian Research Council through the projects RETROSPECT (grant no. 244262) and CIRFA (grant no. 237906). The authors are thankful to W. Koch for preparing the model forcing and A. Behrens for assisting with preparing some of the plots. We are also thankful to the German Federal Maritime and Hydrographic Agency (BSH) for providing the in-situ measurement data.

References

- Aiki H, Greatbatch RJ (2013) The vertical structure of the surface wave radiation stress for circulation over a sloping bottom as given by thickness-weighted-mean theory. *J Phys Oceanogr* 43(1):149–164
- Aiki H, Greatbatch RJ (2014) A new expression for the form stress term in the vertically Lagrangian mean framework for the effect of surface waves on the upper-ocean circulation. *J Phys Oceanogr* 44(1): 3–23
- Alari V, Staneva J, Breivik O, Bidlot JR, Mogensen K and Janssen PAEM (2015) Response of water temperature to surface wave effects in the Baltic Sea: simulations with the coupled NEMO-WAM model. Submitted to *Ocean Dynamics*
- Ardhuin F, Raschle N, Belibassakis K (2008) Explicit wave-averaged primitive equations using a generalized Lagrangian mean. *Ocean Modell.* 20(1):35–60
- Ardhuin F, Marie L, Raschle N, Forget P, Roland A (2009) Observation and estimation of Lagrangian, Stokes and Eulerian currents induced by wind and waves at the sea surface. *J Phys Oceanogr* 39:2820–2838. doi:10.1175/2009JPO4169.1
- Ardhuin F, Rogers E, Babanin AV, Filipot J-F, Magne R, Roland A, van der Westhuysen A, Queffelec P, Lefevre J-M, Aouf L, Collard F (2010) Semiempirical dissipation source functions for ocean waves. Part I: definition, calibration, and validation. *J Phys Oceanogr* 40: 1917–1941
- Babanin AV (2006) On a wave-induced turbulence and a wave-mixed upper ocean layer. *Geophys Res Lett* 33(20):6. doi:10.1029/2006GL027308
- Babanin A (2011) *Breaking and dissipation of ocean surface waves*. Cambridge University Press, Cambridge, p 480
- Babanin AV, Chalikov D (2012) Numerical investigation of turbulence generation in non-breaking potential waves. *J Geophys Res* 117: C00J17. doi:10.1029/2012JC007929
- Babanin AV, Haus BK (2009) On the existence of water turbulence induced by nonbreaking surface waves. *J Phys Oceanogr* 39(10): 2675–2679. doi:10.1175/2009JPO4202.1
- Babanin AV, Chalikov D, Young IR, Savelyev I (2010) Numerical and laboratory investigation of breaking of steep two-dimensional waves in deep water. *J Fluid Mech* 644:433–463
- Barbariol F, Benetazzo A, Carniel S, Sclavo M (2013) Improving the assessment of wave energy resources by means of coupled wave-ocean numerical modeling. *Renew Energ* 60:462–471
- Benetazzo A, Carniel S, Sclavo M, Bergamasco A (2013) Wave-current interaction: effect on the wave field in a semi-enclosed basin. *Ocean Model* 70:152–165

- Bennis A, Ardhuin F (2011) Comments on the depth-dependent current and wave interaction equations: a revision. *J Phys Oceanogr* 41: 2008–2012
- Bertin X, Li K, Roland A, Bidlot JR (2015) The contribution of short-waves in storm surges: two case studies in the Bay of Biscay. *Cont Shelf Res* 96:1–15. doi:10.1016/j.csr.2015.01.005
- Bidlot J-R, Janssen P, Abdalla S (2007) A revised formulation of ocean wave dissipation and its model impact. ECMWF Tech. Memo. 509, Eur. Cent. for Medium-Range Weather Forecasts, Reading
- Bolaños R, Osuna P, Wolf J, Monabiu J, Sanchez-Arcilla A (2011) Development of the POLCOMS-WAM current-wave model. *Ocean Model* 36:102–115
- Bolaños R, Brown JM, Souza AJ (2014) Wave-current interactions in a tide dominated estuary. *Cont Shelf Res* 87:109–123. doi:10.1016/j.csr.2014.05.009
- Bouillon S, Maqueda MA, Legat V, Fichefet T (2009) An elastic-viscous-plastic sea ice model formulated on Arakawa B and C grids. *Ocean Model* 27:174–184
- Breivik Ø, Janssen P, Bidlot JR (2014) Approximate Stokes drift profiles in deep water. *J Phys Oceanogr* 44(9):2433–2445. doi:10.1175/JPO-D-14-0020.1arXiv:1406.5039
- Breivik Ø, Mogensen K, Bidlot JR, Balmaseda MA, Janssen PAEM (2015) Surface wave effects in the NEMO Ocean model: forced and coupled experiments. *Journal of Geoph. Research C: Oceans* 120(4):2973–2992
- Breivik Ø, Bidlot J-R, Janssen PA (2016) A Stokes drift approximation based on the Phillips spectrum. *Ocean Model* 100:49–56. doi:10.1016/j.ocemod.2016.01.005
- Brown JM, Wolf J (2009) Coupled wave and surge modelling for the eastern Irish Sea and implications for model wind-stress. *Cont Shelf Res* 29(10):1329–1342
- Brown JM, Bolaños R, Wolf J (2011) Impact assessment of advanced coupling features in a tide-surge-wave model, POLCOMS-WAM, in a shallow water application. *J Mar Syst* 87(1):13–24
- Brown JM, Bolaños R, Wolf J (2013) The depth-varying response of coastal circulation and water levels to 2D radiation stress when applied in a coupled wave-tide-surge modelling system during an extreme storm. *Coast Eng* 82:102–113
- Charnock H (1955) Wind stress on a water surface. *Q J R Meteorol Soc* 81(350):639–640
- Craig PD, Banner ML (1994) Modeling wave-enhanced turbulence in the ocean surface layer. *J Phys Oceanogr* 24(12):2546–2559
- Davies AM, Kwong SCM, Flather RA (2000) On determining the role of wind wave turbulence and grid resolution upon computed storm driven currents. *Cont Shelf Res* 20:1825–1888
- Dean RG, Dalrymple RA (1991) *Water waves mechanics for engineers and scientists*. World Scientific, London
- Deutschländer T, Friedrich K, Haeseler S and Lefebvre C (2013) Severe storm XAVER across northern Europe from 5 to 7 December 2013, December, 2013 DWD report. Available from <https://www.dwd.de/EN/ourservices/specialevents/storms>
- Dieterich C, Schimanke S, Wang S, Väli G, Liu Y, Hordoir R, Axell L, Hoeglund A, Meier HEM (2013) Evaluation of the SMHI coupled atmosphere-ice-ocean model RCA4-NEMO. *Rep. Oceanogr* 4, 80 pp
- Donelan MA, Curcic M, Chen SS, Magnusson AK (2012) Modeling waves and wind stress. *J Geophys Res* 117: C00J23. doi:10.1029/2011JC007787
- Drennan WM, Donelan MA, Terray EA, Katsaros KB (1996) Oceanic turbulence dissipation measurements in SWADE. *J Phys Oceanogr* 26(5):808–815
- ECMWF (2014) CY40R1 Official IFS Documentation, <https://software.ecmwf.int/wiki/display/IFS/CY41R1+Official+IFS+Documentation>
- Fan Y, Ginis I, Hara T (2009) The effect of wind-wave-current interaction on air-sea momentum fluxes and ocean response in tropical cyclones. *J Phys Oceanogr* 39(4):1019–1034. doi:10.1175/2008JPO4066.1
- Fenoglio-Marc L, Scharroo R, Annunziato A, Mendoza L, Becker M, Lillibridge J (2015) Cyclone Xaver seen by geodetic observations. *Geophys Res Lett* 42:9925–9932. doi:10.1002/2015GL065989
- Flather RA (2001) Storm surges. In: Steele J, Thorpe S, Turekian K (eds) *Encyclopedia of ocean sciences*. Academic, San Diego, pp. 2882–2892
- Grashorn S, Lettmann KA, Wolff J-O, Badewien TH, Stanev EV (2015) East Frisian Wadden Sea hydrodynamics and wave effects in an unstructured-grid model. *Ocean Dyn* 65(3):419–434
- Günther, H, Hasselmann S, Janssen PAEM (1992) The WAM model cycle 4.0. user manual technical report no. 4 Deutsches Klimarechenzentrum, Hamburg, Germany, 102 pages
- Haeseler, S and C Lefebvre (2013) Heavy storm CHRISTIAN on 28 October 2013, DWD report, November, 2013. Available from <https://www.dwd.de/EN/ourservices/specialevents/storms>
- Hasselmann K (1970) Wave-driven inertial oscillations. *Geophys Astrophys Fluid Dyn* 1(3–4):463–502. doi:10.1080/03091927009365783
- Hersbach H, Janssen P (1999) Improvements of the short fetch behaviour in the WAM model. *J Atmos Oceanic Techn* 16:884–892
- Hewson, T, L Magnusson, Ø Breivik, F Prates, I Tsonevsky, H d Vries (2014). Windstorms in northwest Europe in late 2013, European Centre for Medium-Range Weather Forecasts, Newsletter 139, pp 22–28. Available from <https://www.ecmwf.int/en/elibrary/14582-newsletter-no139-spring-2014>
- Hordoir R, An BW, Haapala J, Dieterich C, Schimanke S, Hoeglund A, Meier HEM (2013) A 3D ocean modelling configuration for Baltic & North Sea exchange analysis. *Rep Oceanogr* 48:–72
- Huang CJ, Qiao F, Song Z, Ezer T (2011) Improving simulations of the upper ocean by inclusion of surface waves in the Mellor-Yamada turbulence scheme. *J Geophys Res* 116(C1):C01007. doi:10.1029/2010JC006320
- Janssen P (1991) Quasi-linear theory of wind-wave generation applied to wave forecasting. *J Phys Oceanogr* 21(11):1631–1642. doi:10.1175/1520-0485(1991)021<1631:QLTOWW>2.0.CO;2
- Janssen PAEM (2012) Ocean wave effects on the daily cycle in SST. *J Geophys Res* 117:C00J32. doi:10.1029/2012JC007943201
- Janssen PAEM (1989) Wave-induced stress and the drag of air flow over sea waves. *J Phys Oceanogr* 19:745–754
- Janssen F, Schrum C, Backhaus JO (1999) A climatological data set of temperature and salinity for the Baltic Sea and the North Sea. *Deutsche Hydrographische Zeitschrift* 51(9 Supplement):5–245
- Janssen, PAEM, Breivik, Ø, Mogensen, K, Vitart, F, Balmaseda, M, Bidlot, J-R, Keeley, S, Leutbecher, M, Magnusson, L, Molteni, F, (2013) Air-sea interaction and surface waves, ECMWF. Technical Memorandum 712, 34 pp
- Jones JE, Davies AM (1998) Storm surge computations for the Irish Sea using a three-dimensional numerical model including wave-current interaction. *Cont Shelf Res* 18:201–251
- Katsafados P, Papadopoulos A, Korres G, Varlas G (2016) A fully coupled atmosphere-ocean wave modeling system for the Mediterranean Sea: interactions and sensitivity to the resolved scales and mechanisms. *Geosci Model Dev* 9:161–173. doi:10.5194/gmd-9-161
- Komen GJ, Cavaleri L, Donelan M, Hasselmann K, Hasselmann S, Janssen P (1994) *Dynamics and modelling of ocean waves*. Cambridge University Press, Cambridge 560 pp
- Kumar N, Voulgaris G, Warner JC, Olabarrieta M (2012) Implementation of the vortex force formalism in the coupled ocean-atmosphere-wave-sediment transport (COAWST) modelling system for inner shelf and surf zone applications. *Ocean Model* 47:65–95
- Lamb H, Frydendahl K (1991) *Historic storms of the North Sea*. Cambridge University Press, British Isles and Northwest Europe 208 pages

- Lane EM, Restrepo JM, McWilliams JC (2007) Wave-current interaction: a comparison of radiation-stress and vortex-force representations. *J Phys Oceanogr* 37(5):1122–1141
- Longuet-Higgins MS, Stewart RW (1961) The changes in amplitude of short gravity waves on steady non-uniform currents. *J Fluid Mech* 10:529–549
- Longuet-Higgins MS, Stewart RW (1962) Radiation stress and mass transport in gravity waves, with application to surf beats. *J Fluid Mech* 13:481–504
- Longuet-Higgins MS, Stewart RW (1964) Radiation stresses in water waves: a physical discussion with applications. *Deep-Sea Res* 11: 529–562
- Madec G (2008) NEMO ocean engine. Note du Pole de modelisation. Institut Pierre-Simon Laplace (IPSL), France No. 27, 217 pp
- Mastenbroek C, Burgers G, Janssen PAEM (1993) The dynamical coupling of a wave model and a storm surge model through the atmospheric boundary layer. *J Phys Oceanogr* 23:1856–1866
- McWilliams J, Restrepo J, Lane E (2004) An asymptotic theory for the interaction of waves and currents in coastal waters. *J Fluid Mech* 511:135–178
- Mellor G (2003) The three-dimensional current and surface wave equations. *J Phys Oceanogr* 33(9):1978–1989
- Mellor G, Blumberg A (2004) Wave breaking and ocean surface layer thermal response. *J Phys Oceanogr* 34:693–698
- Mellor G (2005) Some consequences of the three-dimensional current and surface equations. *J Phys Oceanogr* 35(11):2291–2298
- Mellor G (2008) The depth-dependent current and wave interaction equations: a revision. *J Phys Oceanogr* 38(11):2587–2596
- Michaud H, Marsaleix P, Leredde Y, Estoumel C, Bourrin F, Lyard F, Mayet C, Ardhuin F (2012) Three-dimensional modelling of wave-induced current from surf zone to the inner shelf. *Ocean Sci* 8:657–681
- Moghim S, Klingbeil K, Gräwe U, Burchard H (2013) A direct comparison of a depth-dependent radiation stress formulation and a vortex force formulation within a three-dimensional coastal ocean model. *Ocean Model* 70:132–144
- O’Dea EJ, Arnold AK, Edwards KP, Fumer HP, Martin MJ, Siddorn JR, Storkey D, While J, Holt JT, Liu H (2012) An operational ocean forecast system incorporating NEMO and SST data assimilation for the tidally driven European North-West shelf. *J Oper Oceanogr* 5:3–17
- Pawlowicz R, Beardsley B, Lent S (2002) Classical tidal harmonic analysis including error estimates in MATLAB using T-TIDE. *Comput Geosci* 28(8):929–937. doi:10.1016/S0098-3004(02)
- Pham TV, Brauch J, Dieterich C, Frueh B, Ahrens B (2014) New coupled atmosphere-ocean-ice system COSMO-CLM/NEMO: assessing air temperature sensitivity over the North and Baltic seas. *Oceanologia* 56(2):167–189
- Polton JA, Lewis DM, Belcher SE (2005) The role of wave-induced Coriolis-stokes forcing on the wind-driven mixed layer. *J Phys Oceanogr* 35:444–457. doi:10.1175/JPO2701.1
- Röhrs J, Christensen KH, Hole LR, Broström G, Drivdal M, Sundby S (2012) Observation-based evaluation of surface wave effects on currents and trajectory forecasts. *Ocean Dyn* 62:1519–1533
- Röhrs J, Sperrevik AK, Breivik Ø, Broström G, Christensen KH (2015) Comparison of HF radar measurements with Eulerian and Lagrangian surface currents. *Ocean Dyn* 65:679–690. doi:10.1007/s10236-015-0828-8
- Roland A, Cucco A, Ferrarin C, Hsu T, Liao J, Ou S, Umgiesser G, Zanke U (2009) On the development and verification of a 2-D coupled wave-current model on unstructured meshes. *J Mar Syst* 78:244–254
- Stacey MW (1999) Simulations of the wind-forced near-surface circulation in Knight Inlet: a parameterization of the roughness length. *J Phys Oceanogr* 29:1363–1367
- Stokes GG (1847) On the theory of oscillatory waves. *Trans Camb Philos Soc* 8:441–455
- Saetra O, Albretsen J, Janssen P (2007) Sea-state-dependent momentum fluxes for ocean modeling. *J Phys Oceanogr* 37(11):2714–2725. doi:10.1175/2007JPO3582.1
- Siddorn J, Good SA, Harris CM, Lewis HW, Maksymczuk J, Martin MJ, Saulter A (2016) Research priorities in support of ocean monitoring and forecasting at the Met Office. *Ocean Sci* 12:217–231. doi:10.5194/os-12-217-201
- Staneva J, Wahle K, Günther H and Stanev E, (2015) Coupling of wave and circulation models in coastal-ocean predicting systems: a case study for the German Bight, MS No.: OS-2015-86. Special Issue: operational oceanography in Europe 2014 in support of blue and green growth, 12, 3169–3197
- Terray EA, Donelan MA, Agrawal YC, Drennan WM, Kahma KK, Williams AJ, Hwang PA, Kitaigorodskii SA (1996) Estimates of kinetic energy dissipation under breaking waves. *J Phys Oceanogr* 26(5):792–807
- Uchiyama Y, McWilliams J, Shchepetkin A (2010) Wave-current interaction in an oceanic circulation model with a vortex-force formalism: application to the surf zone. *Ocean Modell* 34:16–35
- Viitaka M, Maljutenko I, Alari V, Suursaar U, Rikka S, Lagema P (2016) The impact of surface currents and sea level on the wave field evolution during St. Jude storm in the eastern Baltic Sea. *Oceanologia*. doi:10.1016/j.oceano.2016.01.004
- WAMDI Group (1988) The WAM model—a third generation ocean wave prediction model. *J Phys Oceanogr* 18:1775–1810
- Weber JEH, Brostrom G, Saetra O (2006) Eulerian versus Lagrangian approaches to the wave-induced transport in the upper ocean. *J Phys Oceanogr* 31:2106–2118
- Whitham GB (1974) Linear and nonlinear waves. Wiley, New York
- Wolf J, Brown JM, Bolaños R, Hedges T (2011) Waves in coastal and estuarine waters. In: Wolanski E, McLusky D (eds) *Treatise on estuarine and coastal science*, vol 2. Elsevier, Amsterdam, pp. 171–212